

GENERAL DECLASSIFICATION SCHEDULE

**IN ACCORDANCE WITH
DOD 5200.1-R & EXECUTIVE ORDER 11652**

THIS DOCUMENT IS:

CLASSIFIED BY _____

**Subject to General Declassification Schedule of
Executive Order 11652-Automatically Downgraded at
2 Years Intervals- DECLASSIFIED ON DECEMBER 31, ____.**

BY

**Defense Documentation Center
Defense Supply Agency
Cameron Station
Alexandria, Virginia 22314**

AD

CLASSIFICATION CHANGED

FROM **CONFIDENTIAL** TO **UNCLASSIFIED**

43214

ON 2 March 1955 By authority of Reclass. Bull. List No. 17
Month Day Year Specify Authority Being used

This action was rendered by Arthur E. Creach OSA
Name in full Date

Document Service Center, STIA

7

7

**NOTICE. THIS DOCUMENT CONTAINS INFORMATION AFFECTING THE
NATIONAL DEFENSE OF THE UNITED STATES WITHIN THE MEANING
OF THE ESPIONAGE LAWS, TITLE 18, U.S.C., SECTIONS 793 and 794.
THE TRANSMISSION OR THE REVELATION OF ITS CONTENTS IN
ANY MANNER TO AN UNAUTHORIZED PERSON IS PROHIBITED BY LAW.**

L

L

Artillery Design Data

Ordnance Department

U. S. Army

PRELIMINARY INVESTIGATION OF LOAD
DISTRIBUTION IN THREADED CONNECTIONS
1954

Contract No. DA-11-022-ORD-17

Chicago Ordnance District

Division of Engineering Sciences Laboratory

Purdue Research Foundation

Lafayette, Indiana

WAL 730/562-47

54AA

53321

TABLE OF CONTENTS

Foreword	-	-	-	-	-	-	-	-	11
Introduction	-	-	-	-	-	-	-	-	1
Purpose	-	-	-	-	-	-	-	-	1
Summary	-	-	-	-	-	-	-	-	1
Theoretical Analysis	-	-	-	-	-	-	-	-	1
Experimental Analysis	-	-	-	-	-	-	-	-	2
Theoretical Analysis	-	-	-	-	-	-	-	-	2
Notation	-	-	-	-	-	-	-	-	3
Experimental Analysis	-	-	-	-	-	-	-	-	24
Models Tested	-	-	-	-	-	-	-	-	24
Test Procedure	-	-	-	-	-	-	-	-	24
Experimental Results	-	-	-	-	-	-	-	-	28
Conclusions	-	-	-	-	-	-	-	-	37
Appendix	-	-	-	-	-	-	-	-	38
The Petrographic microscope	-	-	-	-	-	-	-	-	38
Bibliography	-	-	-	-	-	-	-	-	42

FOREWORD

This report was prepared under Contract No. DA-11-022-ORD-17 between Purdue Research Foundation and the Chicago Ordnance District, contracting for the Office of Chief of Ordnance, Washington, D. C.

The contract is being administered in the Purdue Research Foundation by Director G. Stanley Meikle and in the Engineering Schools by Dr. G. A. Hawkins, Dean of Engineering, and Professor R. B. Wiley, Head of the School of Civil Engineering and Engineering Mechanics. It is being directed by Dr. Paul F. Chenea. The laboratory work for this report was supervised by Professor E. O. Stitz. Mr. R. M. Gray extended the theory and made all the mathematical computations required. He likewise performed the tests and analyzed the data in the experimental phase of the program. All machining was done in the Civil Engineering and Engineering Mechanics Machine Shop under the direction of Mr. M. E. Beck.

Throughout the period of work, very valuable direction and technical assistance were received from Mr. J. I. Bluhm of Watertown Arsenal. Timely assistance was also furnished by the personnel of the Chicago Ordnance District in giving advice and arranging contracts.

CONFIDENTIAL

PRELIMINARY INVESTIGATION OF LOAD
DISTRIBUTION IN THREADED CONNECTIONS

INTRODUCTION

In accordance with a proposal submitted to Watertown Arsenal on November 12, 1951, an investigation of threaded connections was initiated at Purdue University. The theoretical solution of this problem was first obtained by D. G. Sopwith in 1948 (1)*. Additional work to include the effect of a tapered connection for improving the load distribution between nut and bolt was published by E. E. Stoeckley and H. J. Macke in 1951 (2). The staff of Watertown Arsenal laboratory recognized that a need existed to extend the theory to include various possible types of nut and bolt combinations used particularly in ordnance components and to check the theory experimentally. Three-dimensional photoelasticity was practically the only experimental means available to make this check. Although the general method is well established, special techniques had to be developed for this particular problem.

PURPOSE

This investigation was undertaken to review the existing theory on threaded connections, to extend it, where possible, to include more specific cases, particularly those used in ordnance components, and finally, to check experimentally the theory, using photoelastic models of threaded connections.

SUMMARY

Theoretical Analysis

In the preliminary stages of this investigation, the papers of Sopwith and Stoeckley were reviewed and checked thoroughly. Some points noted in this review were submitted to Watertown Arsenal in Technical Memorandum P-15, early in 1952. It was found that the theoretical analysis could be extended to include many of the problems involving threaded connections not now discussed in the literature. The analytic results of this study are summarized and the solutions of each independent permutation of the non-tapered connection problem have been included. Results are presented in analytic and graphic form.

* Numbers in parenthesis refer to items of the Bibliography, Page 42.

CONFIDENTIAL

Experimental Analysis

Photoelastic tests of two configurations of threaded connections were completed and analyzed in this investigation; one used a model of standard configuration and the other had a tapered bolt pitch diameter to improve the distribution of load along the thread helix. The intensity of load carried by the teeth was determined experimentally at twenty-nine points along the thread helix and was compared with the theoretical load distribution as shown in Drawings No. P-440-B and P-441-B, Pages 35 and 36. The analysis of the models was accomplished using a petrographic microscope having the same elements as a conventional polariscope, which permitted accurate readings of both fringe orders and stress direction. This instrument is described in detail in the Appendix. The results of the test indicate that the theoretical load distribution agrees very well in overall appearance with the experimental results, but considerable local deviations may occur due to inaccuracies in machining.

THEORETICAL ANALYSIS

Although the work of Sopwith and Stoeckley has already been published, it is desirable to repeat some portions of their work here and to indicate the differences in the analysis for different configurations of threaded connections, as discussed in unpublished "Notes on a Screw Thread Program", by Applied Mechanics Branch, Watertown Arsenal Laboratory (3). Except for those differences, the analysis proceeds in the same manner as for the above authors and the same assumptions and approximations are employed. It consists in determining the relative axial displacement between the threads of the contacting members due to (a) deformations in the threads, (b) deformations in the body of the male and female members caused by the radial pressure component at the line of contact, and (c) radial displacements due to Poisson's Ratio in the bodies of the two members. The rate of change of the sum of these relative axial displacements is then equated to the algebraic sum of the axial elongations of the male and female components in a differential length element. This leads to a second order differential equation whose solution yields the desired load distribution along the length of the thread helix.

Notation

- a = thread pitch
 b = depth of fundamental triangle of thread
 $c = \frac{b + d}{b}$ (for symmetric bolt and nut threads), and
 $= \frac{R_r}{R_c}$ (for non-symmetric bolt and nut threads)
 d = depth of thread
 h = deflection factor for thread
 h_b, h_n = deflection factors for thread of bolt and nut, respectively
 $k = \frac{A_1}{A_1 + A_2}$
 n = number of threads in engagement
 s = distance along thread helix from free face of bolt
 s_1 = value of s at bearing face of nut ($s_1 = \pi Dn$)
 w = intensity of loading per unit length of helix
 w_m = mean value of $w = \frac{P}{s_1}$
 x = proportion of length from free face of nut = $\frac{s_1 - s}{s_1}$
 A = mean cross-sectional area of bolt ($A = \pi \frac{D^2}{4}$)
 A_1, A_2 = cross-sectional area of bolt and nut respectively
 B_1, B_2, B_3 = constants in equation for deflection factor h

- D = mean diameter of thread $D = \frac{D_2 - D_1}{2}$
 D_0 = diameter of hole in bolt (if any)
 D_1 = root diameter of bolt
 D_2 = root diameter of nut
 D_3 = equivalent outside diameter of nut
 E = Young's modulus
 L = length of engagement
 P = total axial load
 P_x = axial load at x
 T = function of β and μ in equation for deflection factor h
 β = semi-angle of thread
 μ = coefficient of friction between bolt and nut threads
 σ = Poisson's Ratio
 ϕ = friction angle
 $\delta, \delta_2, \delta_3$ = displacements due to bending of threads, radial pressures, and Poisson's Ratio effects, respectively
 γ, α = coefficients in differential equations
 θ, λ, U, V = coefficients in the solutions

In this analysis only threads having a symmetrical triangular profile as shown in Figure 1 will be considered. In addition it is assumed that the nut and bolt have the same elastic properties. The analysis can be extended to non-symmetrical triangular profiles such as that of the New American Standard Unified Screw Thread shown in Figure 3. Details of this analysis are considered later.

The relative axial separation between the threads due to bending of the threads is considered first. The intensity of axial load along the thread helix being w , and, including the effect of impending slipping toward the tip of the thread, the load at any point may be resolved into components as shown in Figure 2. This loading, assumed at mid-depth of the thread, may be resolved into a statically equivalent system of loads at the vertex of the fundamental triangular thread plan form, for which solutions may be obtained applying the Theory of Elasticity. From these solutions the displacement of the contact strip (assumed at mid-depth of the thread) is obtained and the relative axial displacement between the threads determined. This displacement is obviously directly proportional to the intensity of loading on the thread helix and is found to have the value (1),

$$\delta_r = 2h \frac{w}{E} = 2(1 - \sigma^2) \left[B_1 \ln c - \frac{c-1}{c} (B_2 + B_3 \frac{c-1}{c}) \right] \frac{w}{E} \quad (1)$$

where $B_1 = \frac{2(\frac{2 \sin 2\beta}{2\beta - \sin 2\beta} + T)}{2\beta + \sin 2\beta}$

$$B_2 = \frac{2}{2\beta - \sin 2\beta} + \frac{1 - 2\sigma}{(1 - \sigma) \sin 2\beta} - 2T \frac{1 - \cos 2\beta}{\sin 2\beta - 2\beta \cos 2\beta}$$

$$B_3 = \frac{2T}{\sin 2\beta - 2\beta \cos 2\beta}$$

$$T = \frac{2}{1 + \cos 2\beta + \mu \sin 2\beta}$$

All configurations of threaded connections considered in this report experience exactly the same axial displacements due to tooth deformations. Hence δ_r has the same form in all cases. The same holds

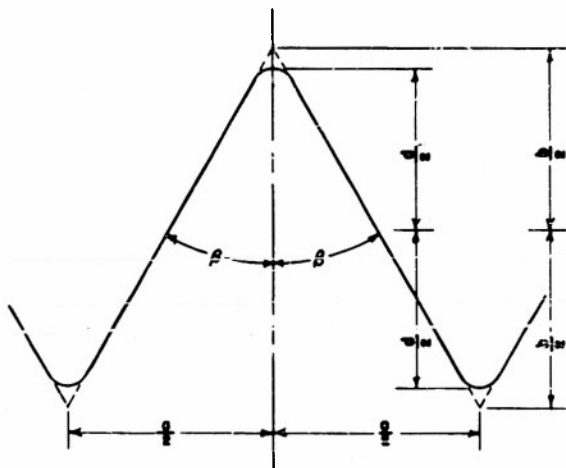


FIG. 1
SYMMETRICAL TRIANGULAR THREAD

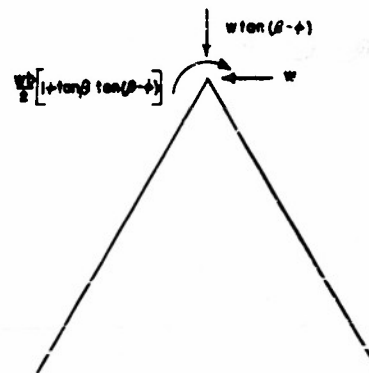


FIG. 2
EQUIVALENT LOAD SYSTEM
FOR TRIANGULAR THREAD

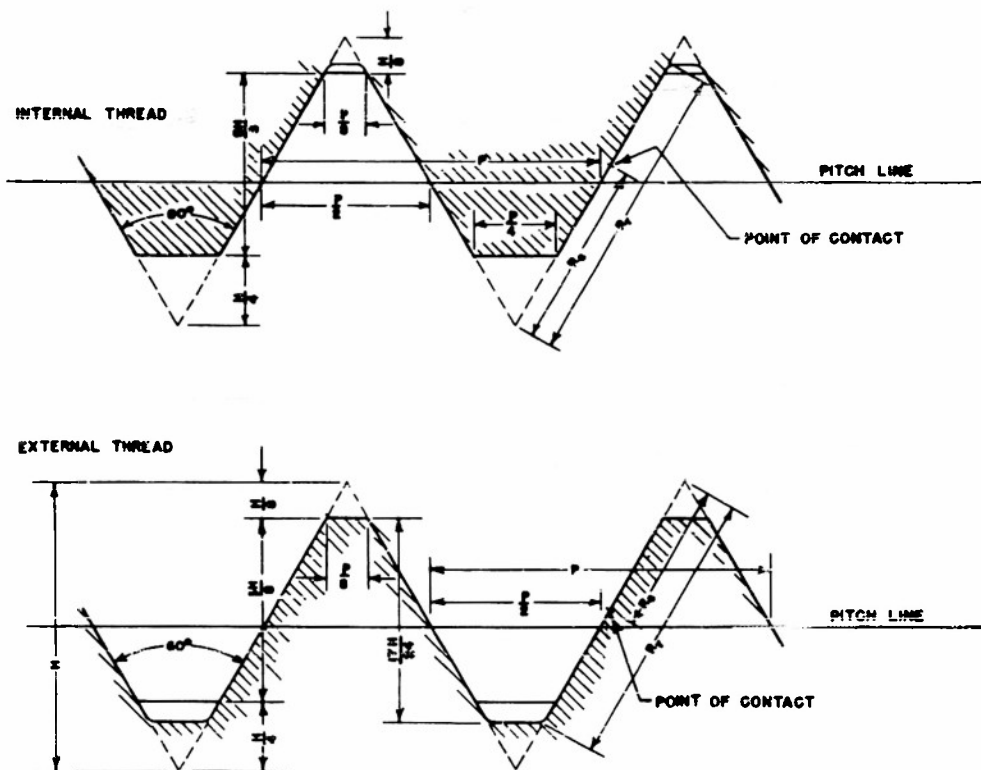


FIG. 3
UNIFIED AND AMERICAN INTERNAL AND EXTERNAL
SCREW THREAD DESIGN FORMS
(MAXIMUM METAL CONDITION)

true for the axial displacements due to radial pressures in the body of the male and female components. From Figure 2 the radial component of force, $w \tan (\beta - \varphi)$, produces a negative radial displacement of the line of contact in the case of the male component and a positive radial displacement in the case of the female component. The net effect is a radial separation of the teeth which in turn causes an axial separation or displacement. Its value, δ_2 , which again is the same for all configurations, is given by:

$$\delta_2 = (k_1 + k_2) \frac{w}{E} = (T - 1) \frac{D}{a} \left(\frac{A}{A_1} + \frac{A}{A_2} \right) \frac{w}{E} \quad (2)$$

Finally the effect of Poisson's Ratio, arising from the axial stresses in the male and female components in producing axial displacement, must be considered. Since this changes between configurations, it will be considered in some detail for each configuration. For reference purposes, the six independent configurations are placed at the head of each of the six lines shown in Figure 4, Page 8. Configurations grouped on any one line have the same load distribution.

(a) Nut in Compression, Bolt in Tension

Taking s as the distance along the thread helix measured from the free end of the bolt (as will be done for all configurations) the axial force in the bolt is $\int_0^s w ds$ tensile and in the nut $\int_0^s w ds$ compression. Then the strain in the radial direction due to Poisson's Ratio is for the bolt and nut respectively

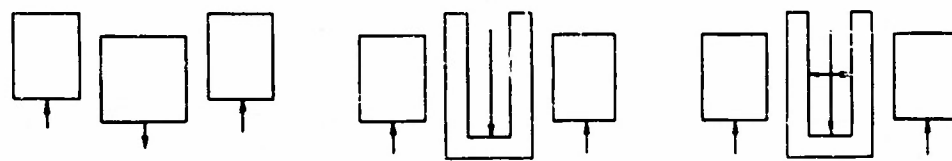
$$- \frac{\sigma \int_0^s w ds}{A_1 E} \quad \text{and} \quad + \frac{\sigma \int_0^s w ds}{A_2 E}$$

This produces radial displacements at the contact strip of:

$$- \frac{D \sigma \int_0^s w ds}{2 A_1 E} \quad \text{and} \quad + \frac{D \sigma \int_0^s w ds}{2 A_2 E}$$

These must be multiplied by $\tan \beta$ to convert from radial displacements to effective axial separations of the contacting teeth and combined. Both produce "relieving" recessions since the teeth tend to become separated in both instances. Thus, we find for the net effect of Poisson's Ratio (with some manipulation)

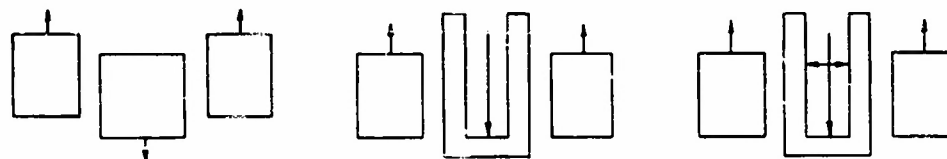
$$\delta_2 = \frac{D \sigma \tan \beta}{2 E} \left(\frac{1}{A_1} + \frac{1}{A_2} \right) \int_0^s w ds = \frac{2 \sigma \tan \beta}{\pi D E} \left(\frac{A}{A_1} + \frac{A}{A_2} \right) \int_0^s w ds \quad (3)$$



SOLUTION (a)



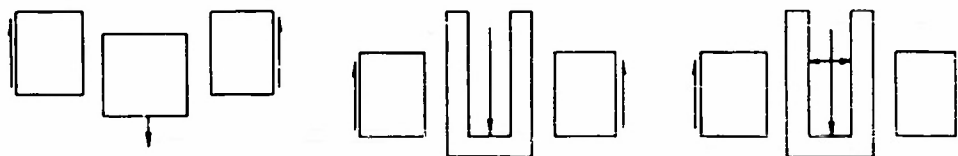
SOLUTION (b)



SOLUTION (c)



SOLUTION (d)



SOLUTION (e)



SOLUTION (f)

Fig. 4 SCHEMATIC DIAGRAMS OF INDEPENDENT PERMUTATIONS TOGETHER WITH THOSE HAVING THE SAME SOLUTIONS

(b) Nut in Tension, Bolt in Compression

In this configuration the effect of Poisson's Ratio is exactly reversed for both the male and female components. It no longer produces a "relieving" recession, but instead, the opposite effect. Hence the sign on δ_3 must be reversed.

$$\delta_3 = - \frac{2\sigma \tan \beta}{\pi D E} \left(\frac{A}{A_1} + \frac{A}{A_2} \right) \int_0^s w ds \quad (4)$$

(c) Nut in Tension, Bolt in Tension

In this configuration the load in the bolt remains the same as before while that in the female component becomes

$$P - \int_0^s w ds$$

In addition, we note the effect of the load in the bolt is to produce a "relieving" recession while that in the female component produces the opposite effect. Hence the net effect is given by

$$\delta_3 = \frac{D \sigma \tan \beta}{2 E} \left[\frac{\int_0^s w ds}{A_1} - \frac{(P - \int_0^s w ds)}{A_2} \right]$$

$$\text{or} \quad \delta_3 = \frac{2\sigma \tan \beta}{\pi D E} \left[\left(\frac{A}{A_1} + \frac{A}{A_2} \right) \int_0^s w ds - \frac{PA}{A_2} \right] \quad (5)$$

(d) Nut in Compression, Bolt in Compression

Again the effect of Poisson's Ratio is found to be reversed to that found in the previous section. Hence

$$\delta_3 = \frac{2\sigma \tan \beta}{\pi D E} \left[\frac{PA}{A_2} - \left(\frac{A}{A_1} + \frac{A}{A_2} \right) \int_0^s w ds \right] \quad (6)$$

(e) Nut in Shear, Bolt in Tension

In this configuration the effect of Poisson's Ratio in the outer component is assumed to be zero. Thus the net effect is given by

$$\delta_3 = \frac{2\sigma \tan \beta}{\pi D E} \frac{A}{A_1} \int_0^s w ds \quad (7)$$

(f) Nut in Shear, Bolt in Compression

For this configuration the effect of Poisson's Ratio in the bolt is reversed from that of the previous one.

$$\delta_3 = - \frac{2\sigma \tan \beta}{\pi D E} \frac{A}{A_1} \int_0^s w ds \quad (8)$$

The axial elongations and contractions of the components are now considered. These might be thought of as "actuating" deformations, since without their effects, the deformations calculated previously would not occur. These effects will also be treated separately for each configuration, since they, too, change depending upon the manner of loading.

(a) Nut in Compression, Bolt in Tension

With s the distance along the thread helix measured from the free end of the bolt, the load in the bolt is:

$$\int_0^s w ds$$

Consequently, in a length dL measured along the length of the bolt, the change in length is:

$$\frac{dL \int_0^s w ds}{A_1 E} = \frac{a}{\pi D} ds \frac{\int_0^s w ds}{A_1 E}$$

Similarly the change in length for the nut is:

$$-\frac{a}{\pi D} ds \frac{\int_0^s w ds}{A_1 E}$$

The difference between the two gives the relative axial movement between the threads of the nut and bolt in a differential length of thread helix.

$$\frac{a}{\pi D E} ds \left(\frac{A}{A_1} + \frac{A}{A_2} \right) \int_0^s w ds$$

(b) Nut in Tension, Bolt in Compression

The amount by which the threads of the bolt and nut are forced together due to the axial load deformations is exactly the same for this configuration as for the previous one.

(c) Nut in Tension, Bolt in Tension

In this configuration the load in the bolt remains the same, while that in the nut becomes:

$$P - \int_0^s w ds$$

This force is tension and the resulting change in length of an element of the nut is positive.

$$\frac{a}{\pi D E} ds \left(\frac{P}{A_2} - \frac{\int_0^s w ds}{A_2} \right)$$

The difference between the two, again giving the relative axial movement between the threads of the nut and bolt, is:

$$\frac{a}{\pi D E} ds \left[\left(\frac{1}{A_1} + \frac{1}{A_2} \right) \int_0^s w ds - \frac{P}{A_2} \right]$$

(d) Nut in Compression, Bolt in Compression

For this configuration the relative movement between the threads is exactly the same as for the previous configuration.

(e) Nut in Shear, Bolt in Tension

The axial deformation of the nut is assumed to be zero for this configuration. Thus only the deformations of the bolt are considered, and the relative movement between the threads is:

$$\frac{a}{\pi D E} ds = \frac{1}{A_1} \int_0^s w ds$$

(f) Nut in Shear, Bolt in Compression

The relative movement between the threads is the same for this configuration as for the one immediately preceding.

The differential equations for each configuration are now obtained by equating the relative axial movement between the threads due to axial loads, to the differentials of the sums of the relative axial displacements due to tooth deformations, radial pressure, and Poisson's Ratio, and then dividing by $\frac{ds}{E}$.

(a) Nut in Compression, Bolt in Tension

$$\frac{a}{\pi D} \left(\frac{1}{A_1} + \frac{1}{A_2} \right) \int_0^s w ds = \frac{d}{ds} (\delta_1 + \delta_2 + \delta_3) = (2h + k_1 + k_2) \frac{dw}{ds} + \frac{2 \sigma \tan \beta}{\pi D} \left(\frac{A}{A_1} + \frac{A}{A_2} \right) w \quad (9)$$

Dividing by $(2h + k_1 + k_2)$ and differentiating with respect to s , the following second order linear differential equation is obtained.

$$\frac{d^2 w}{ds^2} + \frac{\frac{\sigma \tan \beta}{\pi D} \left(\frac{A}{A_1} + \frac{A}{A_2} \right)}{2h + k_1 + k_2} \frac{dw}{ds} - \frac{\frac{a}{\pi D} \left(\frac{1}{A_1} + \frac{1}{A_2} \right)}{2h + k_1 + k_2} w = 0. \quad (10)$$

or
$$\frac{d^2 w}{ds^2} + 2 \gamma \frac{dw}{ds} - \alpha a w = 0, \quad (11)$$

where
$$\alpha = \frac{\frac{1}{\pi D} \left(\frac{1}{A_1} + \frac{1}{A_2} \right)}{2h + k_1 + k_2},$$

$$\gamma = A \sigma \alpha \tan \beta$$

For boundary conditions we have

$$(i) \int_0^{s_1} w ds = P,$$

where $s_1 = \pi D n$

= total length of thread helix.

$$(ii) \left(\frac{dw}{ds} \right)_{s=0} + 2 \gamma w(0) = 0$$

The solution to the above differential equation, subject to the boundary conditions (i) and (ii) is found to be:

$$w = \frac{P e^{\gamma s_1}}{\sinh s_1 \sqrt{\gamma^2 + \alpha a}} e^{-\gamma s} \left[\sqrt{\gamma^2 + \alpha a} \cosh s \sqrt{\gamma^2 + \alpha a} - \gamma \sinh s \sqrt{\gamma^2 + \alpha a} \right] \quad (12)$$

If now we let:

$$w_m = \frac{P}{\pi D n} = \frac{P}{s_1},$$

$$\sqrt{\gamma^2 + \alpha a} s_1 = \theta_2,$$

$$s/s_1 = x,$$

$$\frac{\gamma}{\sqrt{\gamma^2 + \alpha a}} = \lambda,$$

we obtain

$$\frac{w}{w_m} = \frac{\theta_2 e^{\lambda \theta_2 (1-x)}}{\sinh \theta_2} (\cosh \theta_2 x - \lambda \sinh \theta_2 x) \quad (13)$$

where (with some reduction)

$$\theta_2 = \frac{2 L \sqrt{U + V^2}}{U D}$$

$$\lambda = \frac{V}{\sqrt{U + V^2}}$$

$$V = \frac{1}{2} \sigma \tan \beta$$

$$U = \frac{\tan \beta - \mu}{\cot \beta + \mu} + 2 h \frac{a}{D} \frac{(D_3^2 - D^2)(D^2 - D_0^2)}{D^2 (D_3^2 - D_0^2)}$$

For the remaining configurations, only the set-up of equations will be indicated together with boundary conditions and solutions.

(b) Nut in Tension, Bolt in Compression

Differential Equation

$$\frac{a}{\pi D} \left(\frac{1}{A_1} + \frac{1}{A_2} \right) \int_0^s w ds = (2h + k_1 + k_2) \frac{dw}{ds} - \frac{\sigma \tan \beta}{\pi D} \left(\frac{A}{A_1} + \frac{A}{A_2} \right) w \quad (14)$$

$$\text{or} \quad \frac{d^2 w}{ds^2} - 2 \gamma \frac{dw}{ds} - \alpha a w = 0 \quad (15)$$

Boundary Conditions

$$(i) \int_0^s w ds = P$$

$$(ii) \left(\frac{dw}{ds} \right)_{s=0} - 2 \gamma w(0) = 0$$

Solution

$$\frac{w}{w_m} = \frac{\theta_2 e^{-\lambda \theta_2 (x-1)}}{\sinh \theta_2} (\cosh \theta_2 x + \lambda \sinh \theta_2 x) \quad (16)$$

(c) Nut in Tension, Bolt in Tension

Differential Equation

$$\frac{a}{\pi D} \left[\left(\frac{1}{A_1} + \frac{1}{A_2} \right) \int_0^s w ds - \frac{P}{A_2} \right] + (2h + k_1 + k_2) \frac{dw}{ds} + \frac{2 \sigma \tan \beta}{\pi D} \left(\frac{A}{A_1} + \frac{A}{A_2} \right) w \quad (17)$$

$$\text{or} \quad \frac{d^2 w}{ds^2} + 2 \gamma \frac{dw}{ds} - \alpha a w = 0 \quad (18)$$

Boundary Conditions

$$(i) \quad \int_0^s w ds = P$$

$$(ii) \quad \left(\frac{dw}{ds} \right)_{s=0} + 2 \gamma w(0) = - \frac{P a}{\pi D A_2} \frac{1}{2h + k_1 + k_2} = - P a \alpha k$$

Solution

$$\frac{w}{w_m} = \frac{\theta_2 e^{-\lambda \theta_2 x}}{\sinh \theta_2} \left[(1-k) e^{\lambda \theta_2} \left\{ \cosh \theta_2 x - \lambda \sinh \theta_2 x \right\} + k \left\{ \cosh \theta_2 (1-x) + \lambda \sinh \theta_2 (1-x) \right\} \right] \quad (19)$$

$$\text{where} \quad k = \frac{A_1}{A_1 + A_2}.$$

(d) Nut in Compression, Bolt in Compression

Differential Equation

$$\frac{a}{\pi D} \left[\left(\frac{1}{A_1} + \frac{1}{A_2} \right) \int_0^s w ds - \frac{P}{A_2} \right] = (2h + k_1 + k_2) \frac{dw}{ds} - \frac{2\sigma \tan \beta}{\pi D} \left(\frac{A}{A_1} + \frac{A}{A_2} \right) w \quad (20)$$

$$\text{or} \quad \frac{d^2 w}{ds^2} - 2 \bar{\gamma} \frac{dw}{ds} - \bar{\alpha} a w = 0 \quad (21)$$

Boundary Conditions

$$(i) \quad \int_0^s w ds = P$$

$$(ii) \quad \left(\frac{dw}{ds} \right)_{s=0} - 2 \bar{\gamma} w(0) = - \frac{P a}{\pi D A_2} \frac{1}{2h + k_1 + k_2} = - P a \bar{\alpha} k$$

Solution

$$\frac{w}{w_m} = \frac{\theta_2 e^{\lambda \theta_2 x}}{\sinh \theta_2} \left[\frac{(1-k)}{e^{\lambda \theta_2}} \left\{ \cosh \theta_2 x + \lambda \sinh \theta_2 x \right\} + k \left\{ \cosh \theta_2 (1-x) - \lambda \sinh \theta_2 (1-x) \right\} \right] \quad (22)$$

(e) Nut in Shear, Bolt in Tension

Differential Equation

$$\frac{a}{\pi D A_1} \int_0^s w ds = (2h + k_1 + k_2) \frac{dw}{ds} + \frac{2\sigma \tan \beta A}{\pi D A_1} w \quad (23)$$

$$\text{or} \quad \frac{d^2 w}{ds^2} + 2 \bar{\gamma} \frac{dw}{ds} - \bar{\alpha} a w = 0 \quad (24)$$

$$\text{where } \bar{\alpha} = \frac{\frac{1}{\pi D} \cdot \frac{1}{A_1}}{2h + k_1 + k_2}$$

$$\bar{\gamma} = A \sigma \bar{\alpha} \tan \beta$$

Boundary Conditions

$$(i) \int_0^s w ds = P$$

$$(ii) \left(\frac{dw}{ds} \right)_{s=0} + 2 \bar{\gamma} w(0) = 0$$

Solution

$$\frac{w}{w_m} = \frac{\bar{\theta}_2 e^{\bar{\lambda} \bar{\theta}_2 (1-x)}}{\sinh \bar{\theta}_2} \left[\cosh \bar{\theta}_2 x - \bar{\lambda} \sinh \bar{\theta}_2 x \right] \quad (25)$$

where $\bar{\theta}_2$ and $\bar{\lambda}$ are obtained in the same manner as θ_2 and λ with the exceptions:

$$(1) \bar{U} = \frac{\tan \beta - \mu}{\cot \beta + \mu} \left(\frac{D_3^2 - D_o^2}{D_3^2 - D^2} \right) + 2h \frac{a}{D} \left(\frac{D^2 - D_o^2}{D^2} \right)$$

$$(2) \text{ If } D_3 \rightarrow \infty$$

$$\bar{U} = \frac{\tan \beta - \mu}{\cot \beta + \mu} + 2h \frac{a}{D} \frac{D^2 - D_o^2}{D^2}$$

(f) Nut in Shear, Bolt in Compression

Differential Equation

$$\frac{a}{\pi D A_1} \int_0^s w ds = (2h + k_1 + k_2) \frac{dw}{ds} - \frac{2 \sigma \tan \beta A}{\pi D A_1} w \quad (26)$$

or
$$\frac{d^2 w}{ds^2} - 2 \bar{\gamma} \frac{dw}{ds} - \bar{\alpha} a w = 0 \quad (27)$$

Boundary Condition

$$(i) \int_0^s w ds = P$$

$$(ii) \left(\frac{dw}{ds} \right)_{s=0} - 2 \bar{\gamma} w(0) = 0$$

Solution

$$\frac{w}{w_m} = \frac{\bar{\theta}_2 e^{-\bar{\lambda} \bar{\theta}_2 (1-x)}}{\sinh \bar{\theta}_2} (\cosh \bar{\theta}_2 x + \bar{\lambda} \sinh \bar{\theta}_2 x) \quad (28)$$

The theoretical analysis, as presented here, includes all independent configurations of threaded connectors having constant cross-sections, including those with internal pressure in the male component. The only effect of internal pressure is to reduce uniformly the clearance between the nut and bolt threads and thus it does not affect the load distribution. For reference purposes the configurations having the same load distribution are shown in Figure 4.

In order to illustrate the theoretical load distribution for the various configurations, the Unified and American internal and external screw thread design form (maximum metal condition) was selected. The thread forms are shown in Figure 3.* (4) The foregoing analysis applies only in cases where the thread forms on the nut and bolt are exactly alike. Thus it can be assumed that the nut and bolt threads deform in the same manner and that contact occurs at mid-depth of the fundamental triangle. The Unified interior and exterior forms are not alike and the analysis must be modified slightly to include such thread forms. It was assumed that the nut and bolt threads became deformed in such a manner that contact occurred at a point midway between crests of mating teeth, rather than at mid-depth of the fundamental triangle. Such an assumption merely modifies the value of "c" for both the nut and bolt threads and necessitates calculation of two values of h (h_b and h_n). In the equation for "U", we replace $2h$ by $(h_b + h_n)$. The values for "c" are obtained by taking the ratio of the distance from the tip of the fundamental triangle to the bottom of the thread root (measured along the flank of the tooth) to the distance to the point of contact between teeth measured from the same point and in the same manner. Thus "c" may be defined as: (See Figure 3)

$$c = \frac{R_r}{R_c}$$

For the Unified thread, values were obtained as follows:

	$c_b = \frac{40}{21}$	$c_n = \frac{160}{99}$	
For $\mu = .1$	$h_b = 1.656$	$h_n = 1.185$	
For $\mu = .3$	$h_b = 1.572$	$h_n = 1.098$	

* See Page 6

For the one-inch diameter coarse thread series, the following data were used:

$$\begin{array}{ll} D = .9188 & a = .125 \\ D_o = 0 & D_3 = 1.75 \text{ (approximate diameter of a} \\ & \text{circle whose area is equal} \\ & \text{to the gross area of a} \\ & \text{standard nut)} \\ L = 1 & \end{array}$$

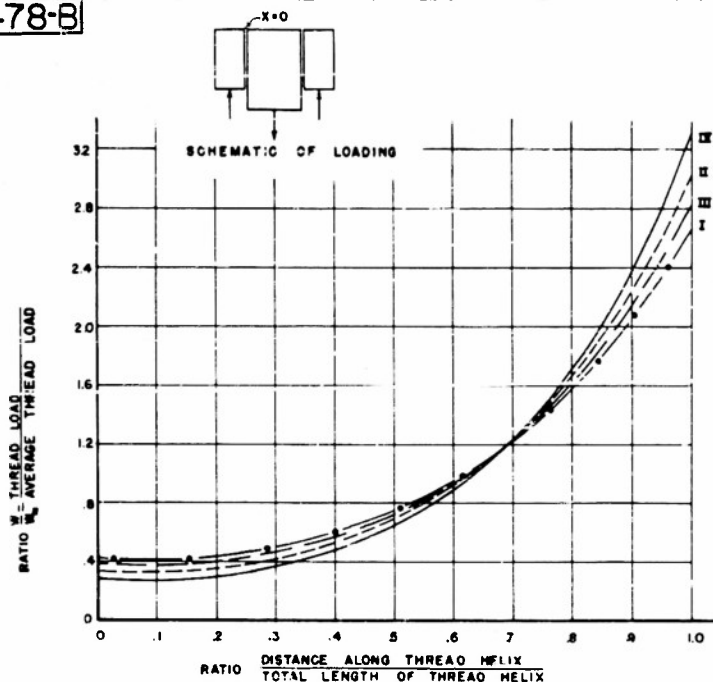
$$\begin{array}{lll} \text{Thus for } \mu = .1 & \lambda = .1112 & \theta_2 = 2.979 \\ \mu = .3 & \lambda = .1291 & \theta_2 = 3.473 \end{array}$$

For the fine thread series the following data were used:

$$\begin{array}{lll} D = .9459 & a = .98333 & \\ L = 1 & D_o = 0 & D_3 = 1.75 \\ \text{Hence for } \mu = .1 & \lambda = .1234 & \theta_2 = 3.220; \\ \text{for } \mu = .3 & \lambda = .1478 & \theta_2 = 3.884. \end{array}$$

The theoretical load distributions for the various independent configurations of threaded connectors are displayed in Drawings P-478-B through P-483-B. In addition, a comparison between configurations may be found in Drawing P-484-B.

P-478-B



ALTERATIONS

MARK	DESCRIPTION	BY	DATE	APPRO

GENERAL NOTES

1. NUT IN COMPRESSION - BOLT IN TENSION
2. CURVE I 1"-8UNC $\mu = .1$
- CURVE II 1"-8UNC $\mu = .3$
- CURVE III 1"-12UNF $\mu = .1$
- CURVE IV 1"-12UNF $\mu = .3$

REFERENCES

$$\frac{W}{W_A} = \frac{e^{a(1-x)} - 1}{\sinh a} [\cosh ax - x \sinh ax]$$

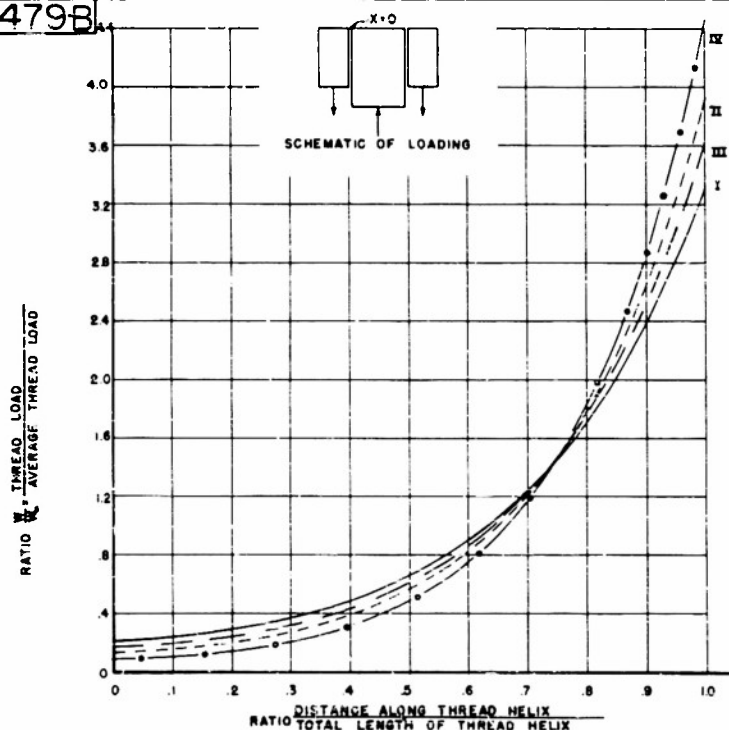
ENGINEERING MECHANICS
LABORATORY
PURDUE UNIVERSITY
PROJECT

LOAD DISTRIBUTION ALONG THREAD HELIX (A)

DRAWN	AS	DATE	7-31-55
CHECKED	AS		
APPROVED	AS		

P-478-B

P-479-B



ALTERATIONS

MARK	DESCRIPTION	BY	DATE	APPRO

GENERAL NOTES

1. NUT IN TENSION - BOLT IN COMPRESSION
2. CURVE I 1"-8UNC $\mu = .1$
- CURVE II 1"-8UNC $\mu = .3$
- CURVE III 1"-12UNF $\mu = .1$
- CURVE IV 1"-12UNF $\mu = .3$

REFERENCES

$$\frac{W}{W_A} = \frac{e^{a(1-x)} - 1}{\sinh a} [\cosh ax + x \sinh ax]$$

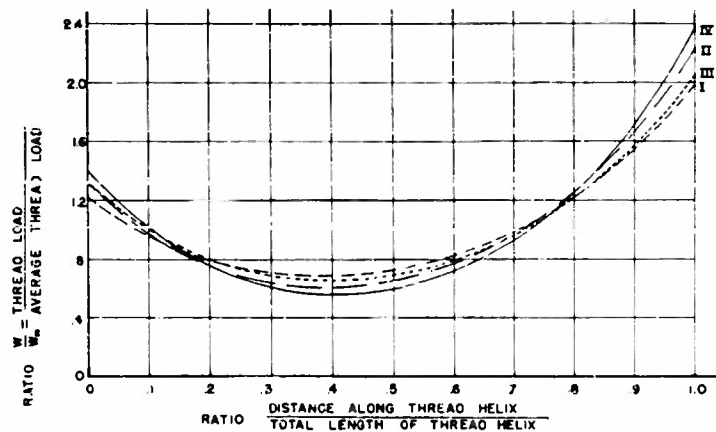
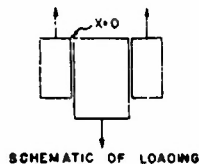
ENGINEERING MECHANICS
LABORATORY
PURDUE UNIVERSITY
PROJECT

LOAD DISTRIBUTION ALONG THREAD HELIX (B)

DRAWN	AS	DATE	7-31-55
CHECKED	AS		
APPROVED	AS		

P-479-B

P-480-B



ALTERATIONS

MARK	DESCRIPTION	BY	DATE	APPRO

GENERAL NOTES

1. NUT IN TENSION - BOLT IN TENSION
2. CURVE I 1"-8UNC $\mu = .1$
- CURVE II 1"-8UNC $\mu = .3$
- CURVE III 1"-12UNF $\mu = .1$
- CURVE IV 1"-12UNF $\mu = .3$

REFERENCES

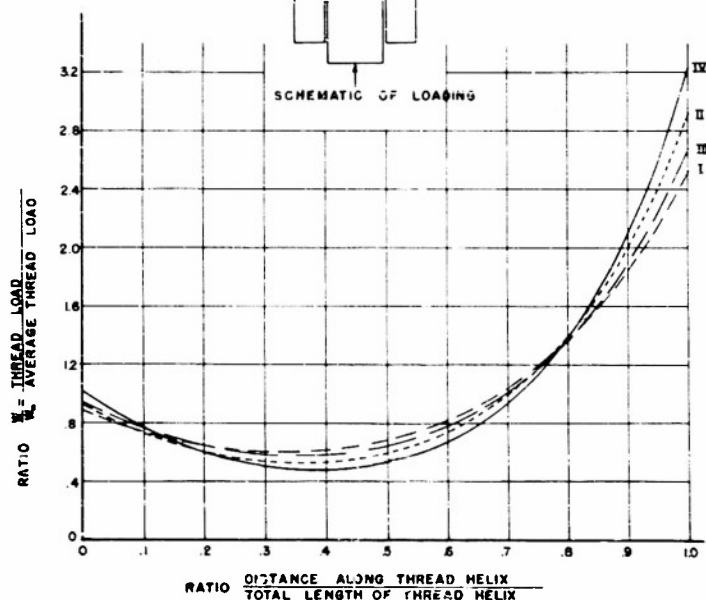
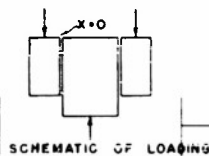
$$W = \frac{\theta_0 e^{-\theta_0 x}}{\sinh \theta_0} \left[(1 - K) e^{-\theta_0 x} \left(\cosh \theta_0 x + \lambda \sinh \theta_0 x \right) + K \left(\cosh \theta_0 (1-x) + \lambda \sinh \theta_0 (1-x) \right) \right]$$

ENGINEERING MECHANICS
LABORATORY
PURDUE UNIVERSITY
PROJECT

LOAD DISTRIBUTION ALONG
THREAD HELIX (C)

DRAWN: *[Signature]* DATE: 7-21-66
CHECKED: *[Signature]*
APPROVED: *[Signature]* P-480-B

P-481-B



ALTERATIONS

MARK	DESCRIPTION	BY	DATE	APPRO

GENERAL NOTES

1. NUT IN COMPRESSION - BOLT IN COMPRESSION
2. CURVE I 1"-8UNC $\mu = .1$
- CURVE II 1"-8UNC $\mu = .3$
- CURVE III 1"-12UNF $\mu = .1$
- CURVE IV 1"-12UNF $\mu = .3$

REFERENCES

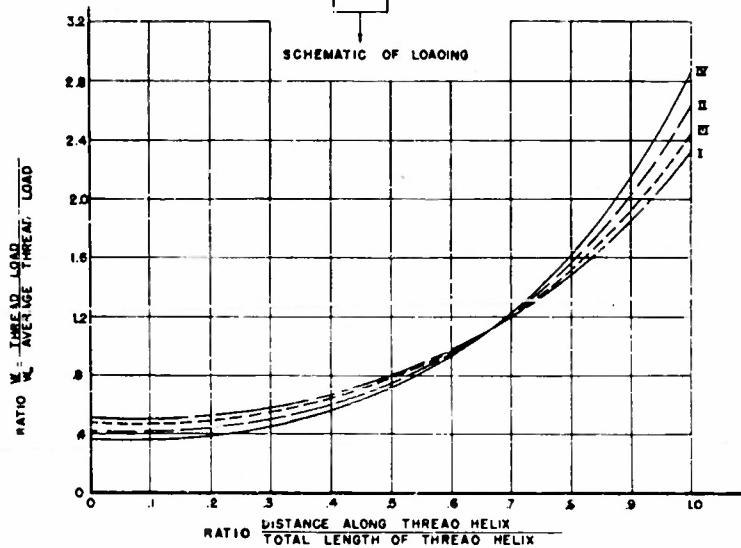
$$W = \frac{\theta_0 e^{-\theta_0 x}}{\sinh \theta_0} \left[(1 - K) e^{-\theta_0 x} \left(\cosh \theta_0 x + \lambda \sinh \theta_0 x \right) + K \left(\cosh \theta_0 (1-x) + \lambda \sinh \theta_0 (1-x) \right) \right]$$

ENGINEERING MECHANICS
LABORATORY
PURDUE UNIVERSITY
PROJECT

LOAD DISTRIBUTION ALONG
THREAD HELIX (D)

DRAWN: *[Signature]* DATE: 7-21-66
CHECKED: *[Signature]*
APPROVED: *[Signature]* P-481-B

P-482-B



ALTERATIONS

MARK	DESCRIPTION	BY	DATE	APPD

GENERAL NOTES

1. NUT IN SHEAR - BOLT IN TENSION
2. CURVE I 1"-8UNC $\mu = 0.1$
- CURVE II 1"-8UNC $\mu = 0.3$
- CURVE III 1"-12UNF $\mu = 0.1$
- CURVE IV 1"-12UNF $\mu = 0.3$

REFERENCES

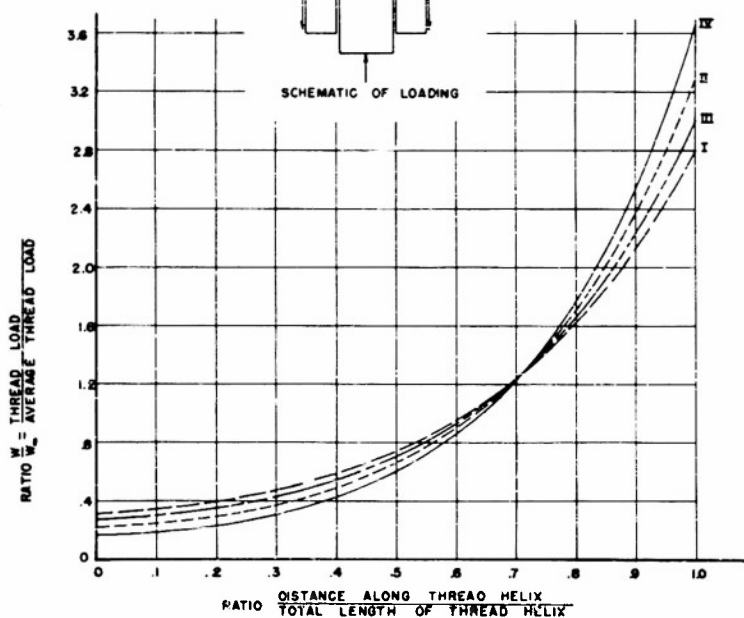
$$\frac{W}{W_a} = \frac{2e^{i\mu\theta}}{\sinh \theta} [\cosh \theta x - \lambda \sinh \theta x]$$

ENGINEERING MECHANICS
LABORATORY
PURDUE UNIVERSITY
PROJECT

LOAD DISTRIBUTION ALONG
THREAD HELIX (E)

DRAWN: *[Signature]* DATE: 7-8-82
CHECKED: *[Signature]*
APPROVED: *[Signature]* P-482-B

P-483-B



ALTERATIONS

MARK	DESCRIPTION	BY	DATE	APPD

GENERAL NOTES

1. NUT IN SHEAR - BOLT IN COMPRESSION
2. CURVE I 1"-8UNC $\mu = 0.1$
- CURVE II 1"-8UNC $\mu = 0.3$
- CURVE III 1"-12UNF $\mu = 0.1$
- CURVE IV 1"-12UNF $\mu = 0.3$

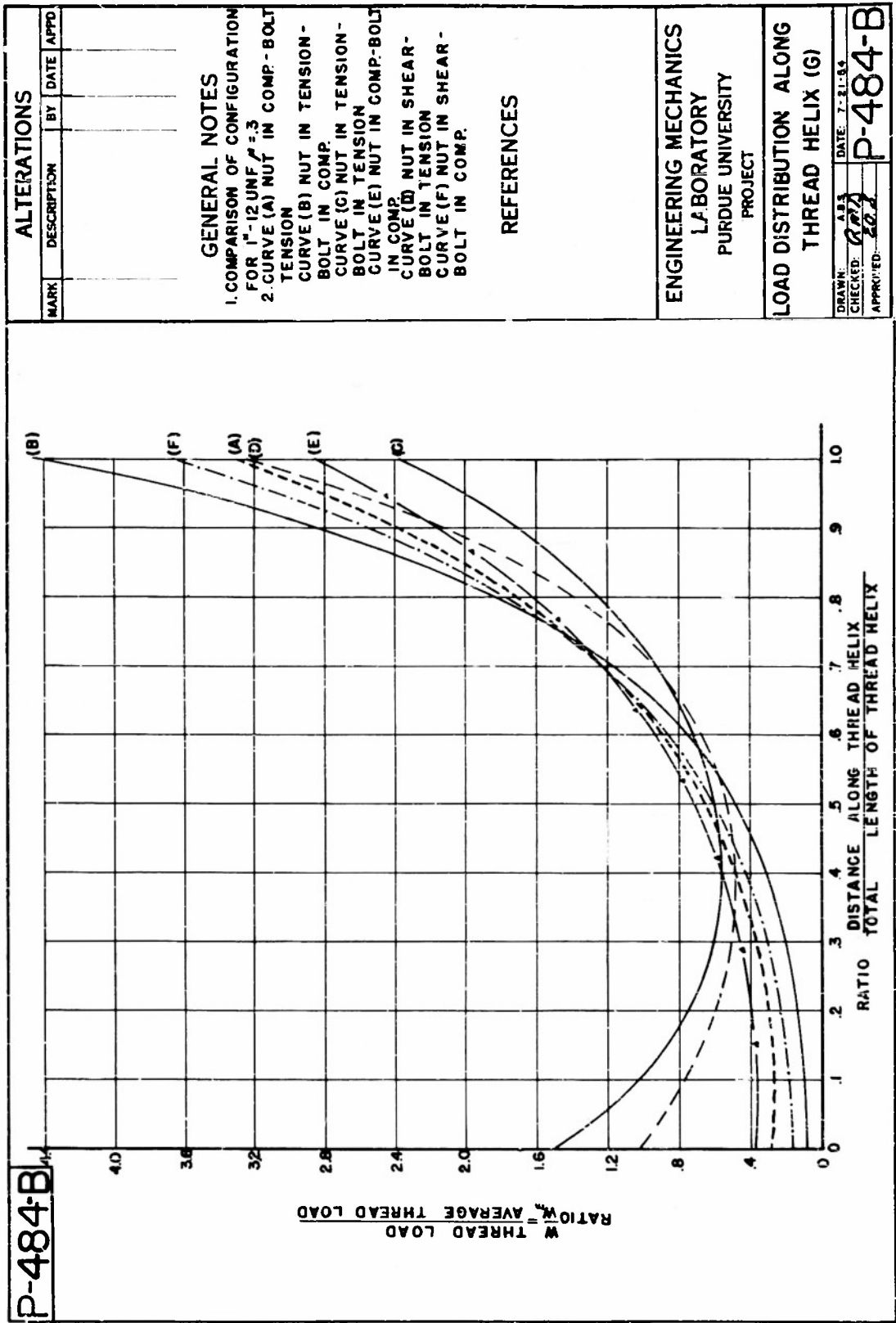
REFERENCES

$$\frac{W}{W_a} = \frac{2e^{i\mu\theta}}{\sinh \theta} [\cosh \theta x + \lambda \sinh \theta x]$$

ENGINEERING MECHANICS
LABORATORY
PURDUE UNIVERSITY
PROJECT

LOAD DISTRIBUTION ALONG
THREAD HELIX (F)

DRAWN: *[Signature]* DATE: 7-8-82
CHECKED: *[Signature]*
APPROVED: *[Signature]* P-483-B



EXPERIMENTAL ANALYSIS

Models Tested

Two photoelastic nut and thread combinations of Fosterite were tested at the same time. Figure 5, Page 25, shows photographs of the model and the test set-up. Drawing P-371-3 gives the detailed dimensions of the model. The thread profiles were the same for both models, having a sixty (60) degree included apex angle and 1/32 inch fillet radii, with a pitch of one-quarter of an inch. The nuts were exactly the same for each model, having a length of two inches, an outside diameter of three and one-half inches, and a thread pitch diameter of 1.791 inches.

The two models differed only in their bolt threads. One had a constant thread pitch diameter of 1.789 inches while the other had a pitch diameter tapered at 0.036 inches per inch. Thus contact between nut and bolt threads occurred initially at the "free end" and progressed along the length of the thread helix as load was applied and the threads deformed.

Test Procedure

The photoelastic models were heated to 70° C. in an oil bath furnace and loaded at that temperature. The load of 46.5 lbs. remained on the model as the temperature was reduced to room temperature and the stresses "frozen in" the model. Following the stress-freezing cycle, four axial slices were cut from the nut and bolt combinations at 90 degrees to one another around the bolt. Care was taken during the slicing process to avoid disturbing the photoelastic patterns which were frozen into the model.

The four slices from each model were analyzed by determining the variation of fringe orders and isoclinics along a line tangent to the base of the threads. The fringe order was a measure of the secondary principal stress difference in a plane containing the axis of the bolt, while the isoclinics gave the direction of one of these secondary principal stresses in the same plane. Using these data, the shear stress component parallel to the axis of the bolt was calculated along the root of the threads, using the relation

$$S_s = \left(\frac{p - q}{2} \right) \sin 2\theta = \frac{nf}{2t} \sin 2\theta$$

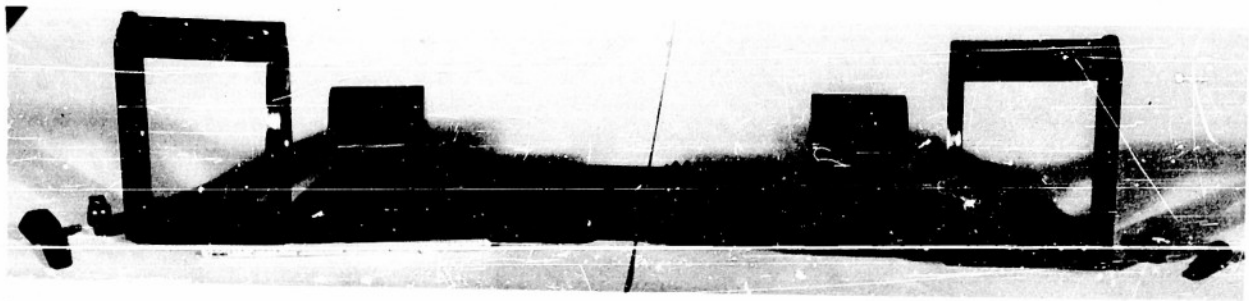


Fig. 5 (a) Detailed View of Screw Thread Model and Loading Jig

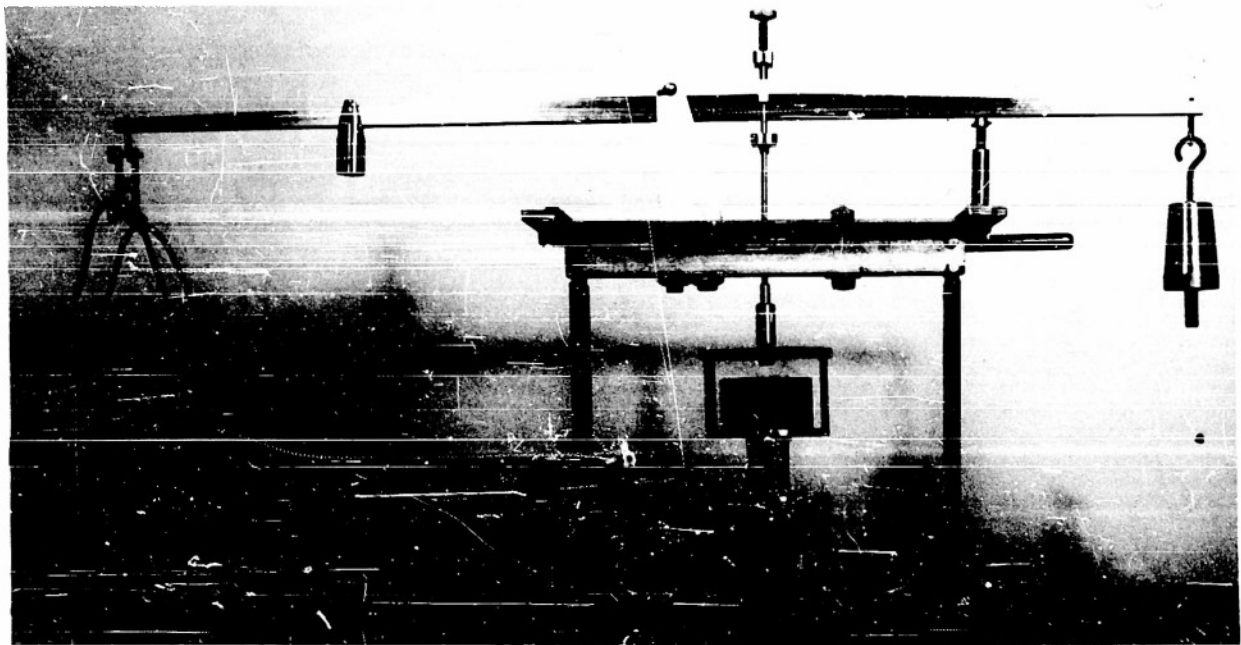
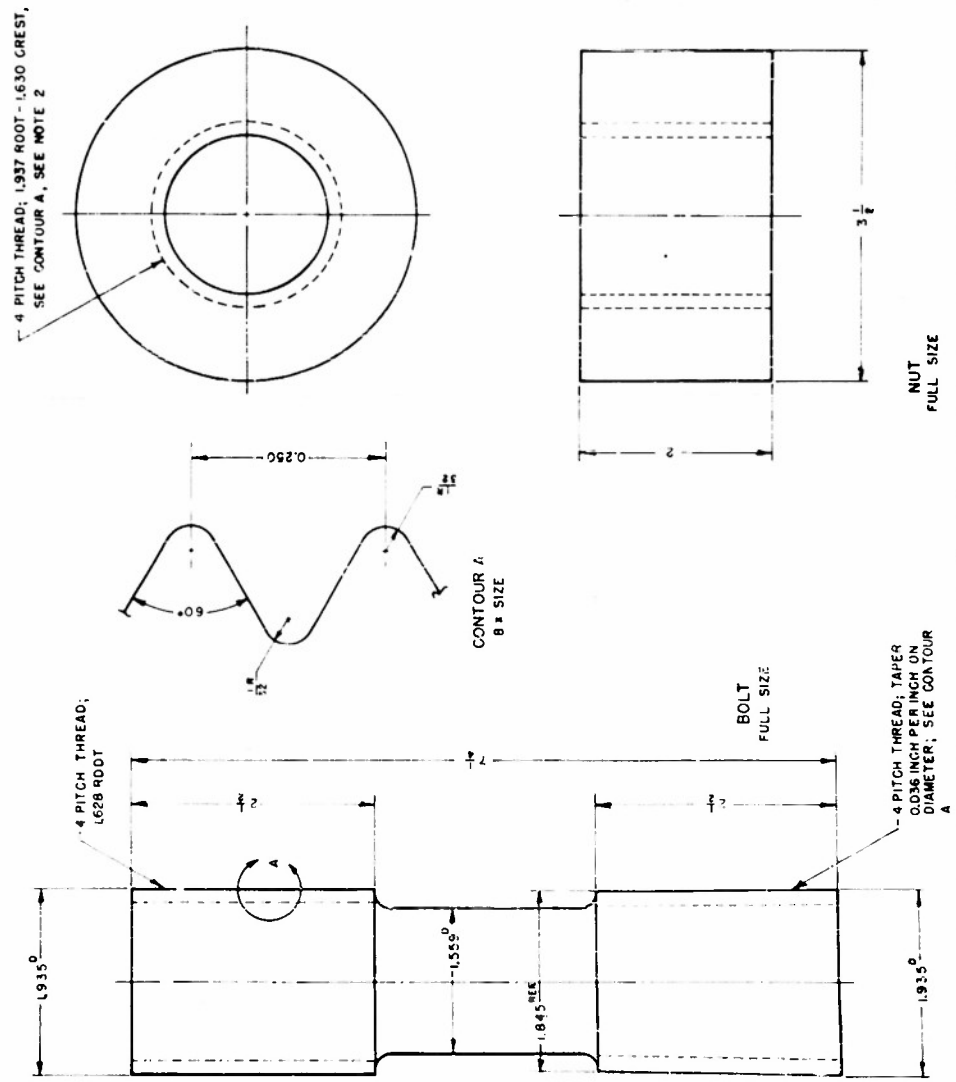


Fig. 5 (b) Loading Frame with Model Ready for Testing

P-371-B

ALTERATIONS			
MARK	DESCRIPTION	BY	DATE



GENERAL NOTES

1. MATERIAL - FOSTERITE
2. PARTIAL THREADS REMOVED TO FIRST COMPLETE THREAD
3. 2 NUTS REQUIRED, 1 BOLT REQUIRED
4. BOLT PITCH DIAMETER, 1.782 (FOR REFERENCE)
5. NUT PITCH DIAMETER, 1.784 (FOR REFERENCE)

REFERENCES

ENGINEERING MECHANICS
LABORATORY
PURDUE UNIVERSITY
PROJECT G-71

PHOTOELASTIC THREAD
MODEL NO. 1

DESIGNED: R.M.G.
DRAWN: S.A.C.
CHECKED: *[Signature]*
APPROVED: *[Signature]*

SCALE: AS MARKED
DATE: 6-7-52

P-371-B

where

- n = the fringe order at any given point
- f = the material fringe constant of the material
- t = the thickness of the slice
- θ = the angle made by one of the principal stresses to the axis of the bolt.

It is easily seen that $\int S_s dA = \int S_s t dy$, where the integration is performed across the base of one tooth, gives a measure of the total force carried on the tooth of a particular slice, while

$$\frac{1}{t} \int S_s t dy$$

is a measure of the intensity of this load along the thread helix. The preceding load intensity was divided by the average load intensity

$$\frac{P}{n \pi D}$$

to reduce it to a non-dimensional form and then plotted versus proportion of length of thread helix.

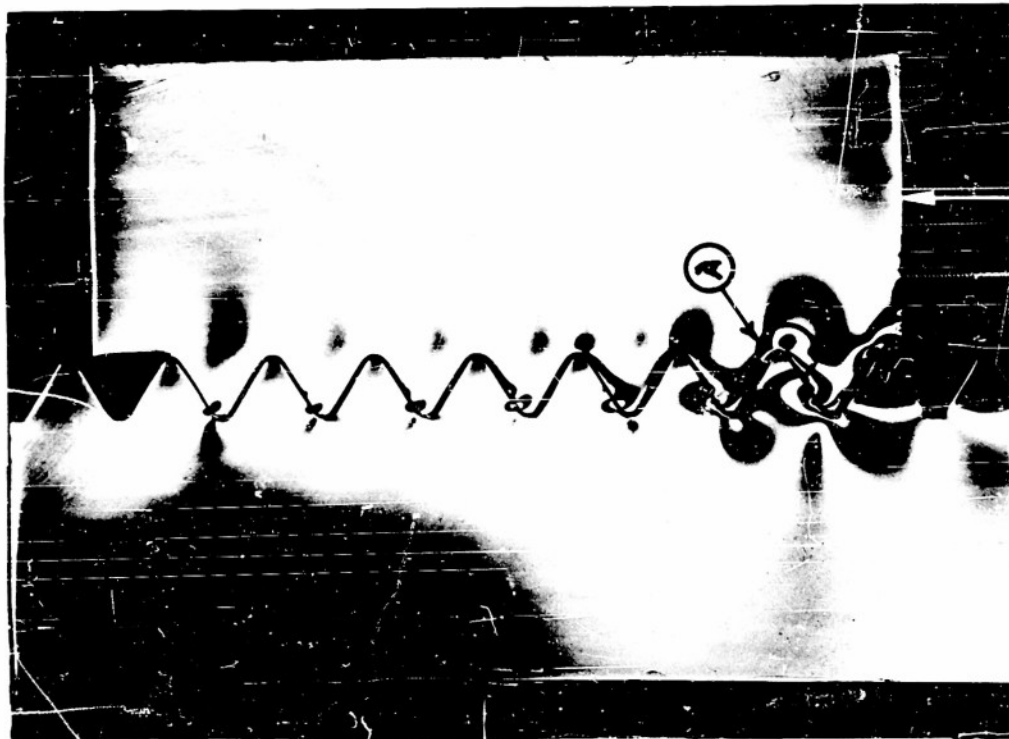
EXPERIMENTAL RESULTS

Photoelastic fringe photographs of slices from the two models are shown in Figures 6 and 7, Pages 29 and 30. It will be observed that a relatively high fringe (proportional to the maximum shear stress) occurs near the root of the thread in every case. Close examination reveals that this high shear stress occurs a finite distance beneath the root of the thread and not at the surface of the thread root. (See Figure 6, Page 31). In fact the tangential stress at a point near the bottom of the root fillet is zero in every case except at the end thread. The gradient of stress in every direction away from that point is, however, very high, and reaches its maximum in a direction toward the point of maximum fringe order mentioned above.

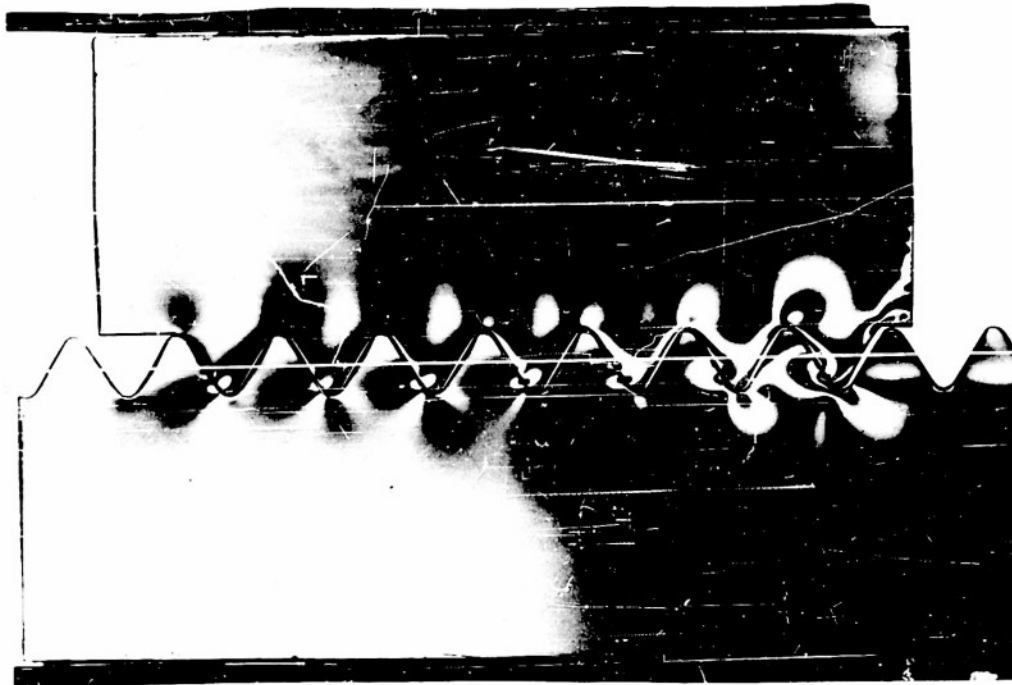
It was first believed that the maximum shear stress mentioned in the previous paragraph would be a suitable indication of the load carried on any tooth profile. That this is not true becomes apparent immediately if we consider that it is sensitive to the point of application of load on the tooth profile. In that case it would not be a suitable indicator for the tapered thread model, since in the latter case the point of application of load quite obviously varied from one tooth to the next. In addition, the high value of shear stress arises due to the interaction of stresses from the two adjacent threads. Thus it is not a direct measure of the load carried on either of the two adjacent threads.

For the above reasons it was necessary to evaluate the total shearing force at the base of each thread in order to obtain a measure of the total force carried by the thread. This was done by calculating the shearing stress on planes tangent to the root of the threads and integrating numerically. The shearing stress was calculated from readings of the fringe (proportional to the maximum shear) and the stress direction. Some difficulty was experienced in getting accurate values of both.

The preceding readings were taken at approximately 25 points along the base of each thread using a petrographic microscope, modified for photoelastic use, which permitted accurate readings of fringe order and stress directions (isoclinics). (See Appendix A for description of the petrographic microscope).

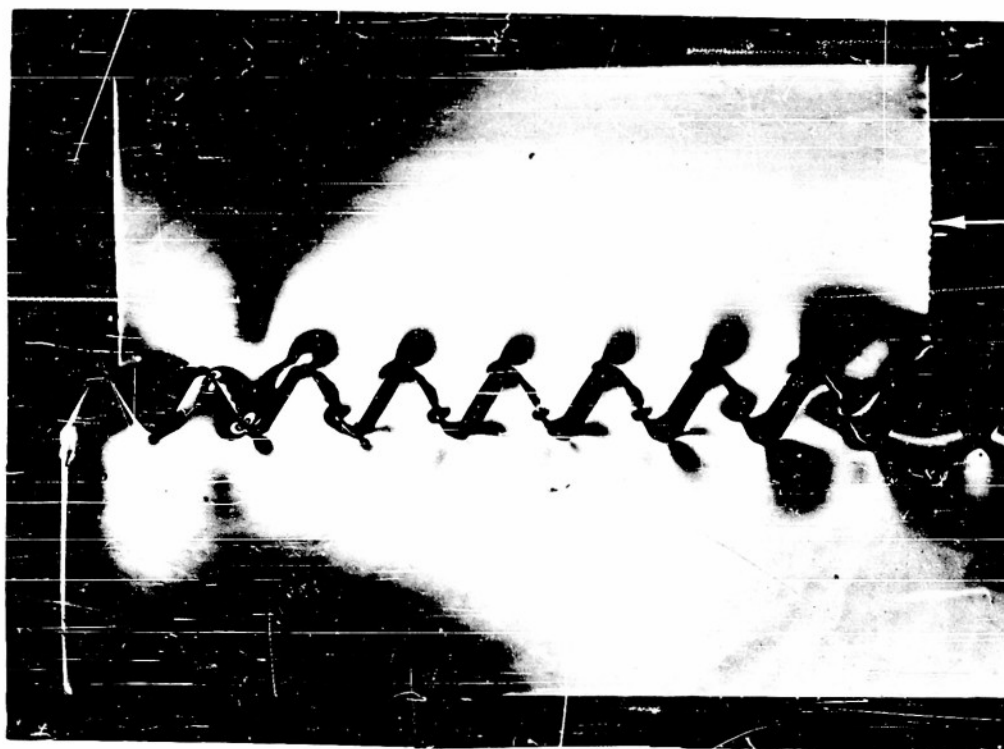


(a) Dark Field

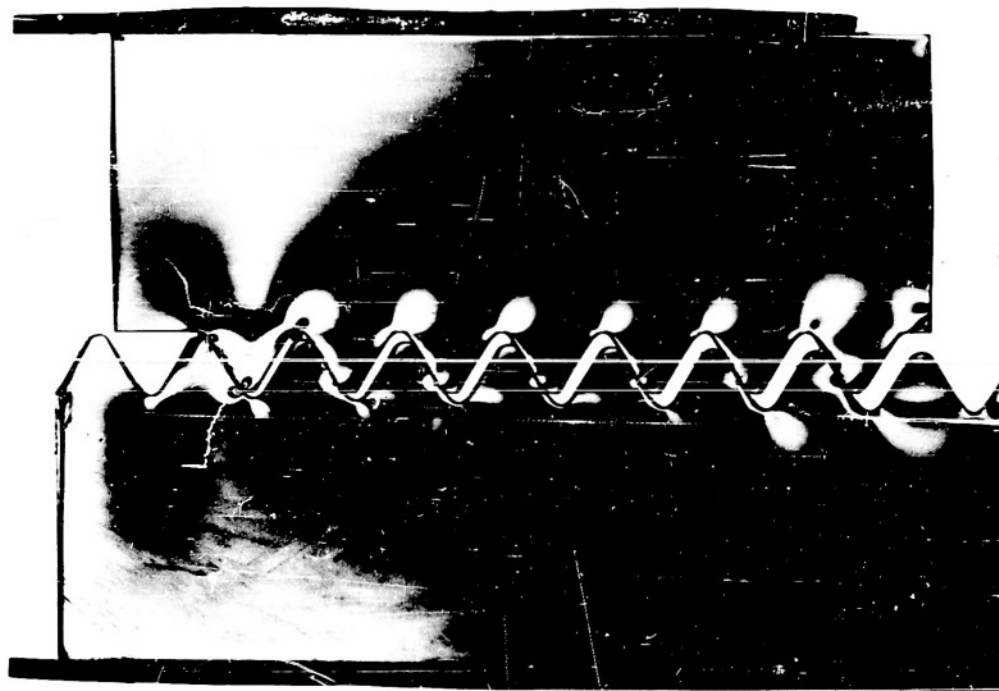


(b) Light Field

Fig. 6 Photoelastic Pattern of Non-Tapered Screw Thread - Slice No. 5
Material, Fosterite
Thickness, 0.135"



(a) Dark Field



(b) Light Field

Fig. 7 Photoelastic Patterns of Tapered Screw Thread Model - Slice No. 3
Material, Fosterite
Thickness, 0.130"

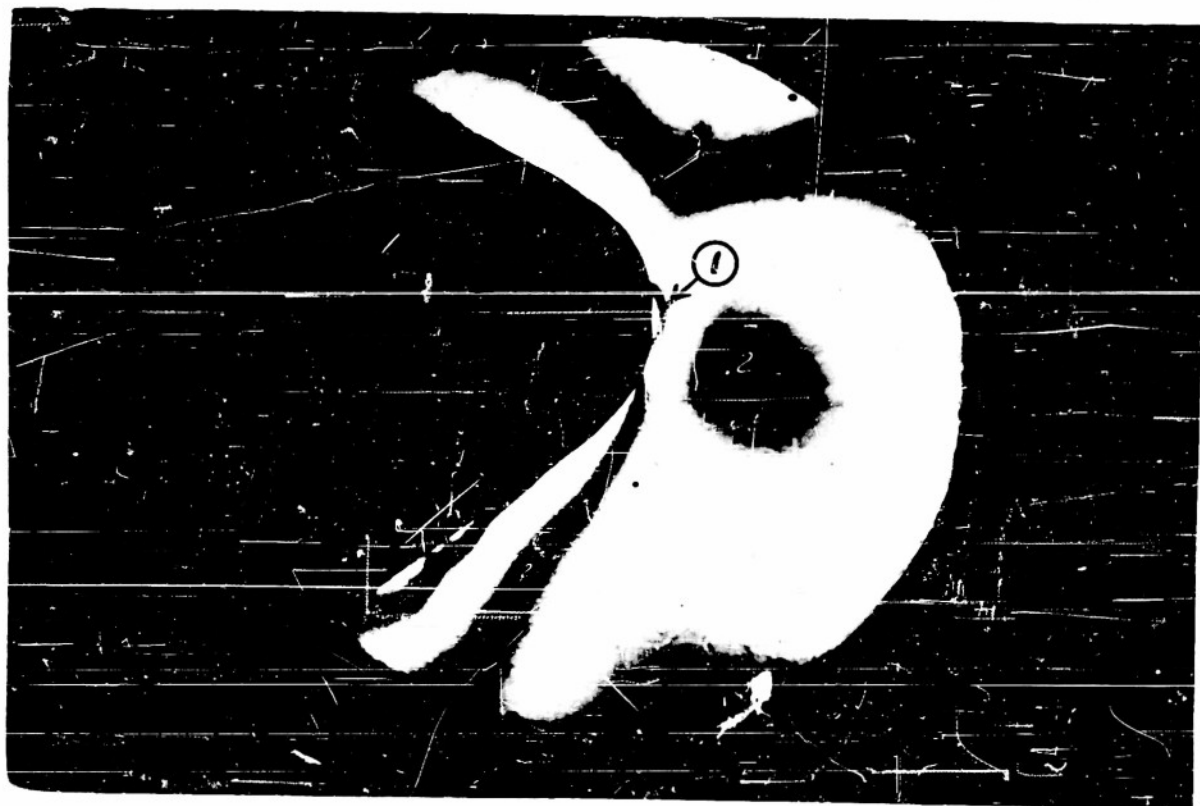


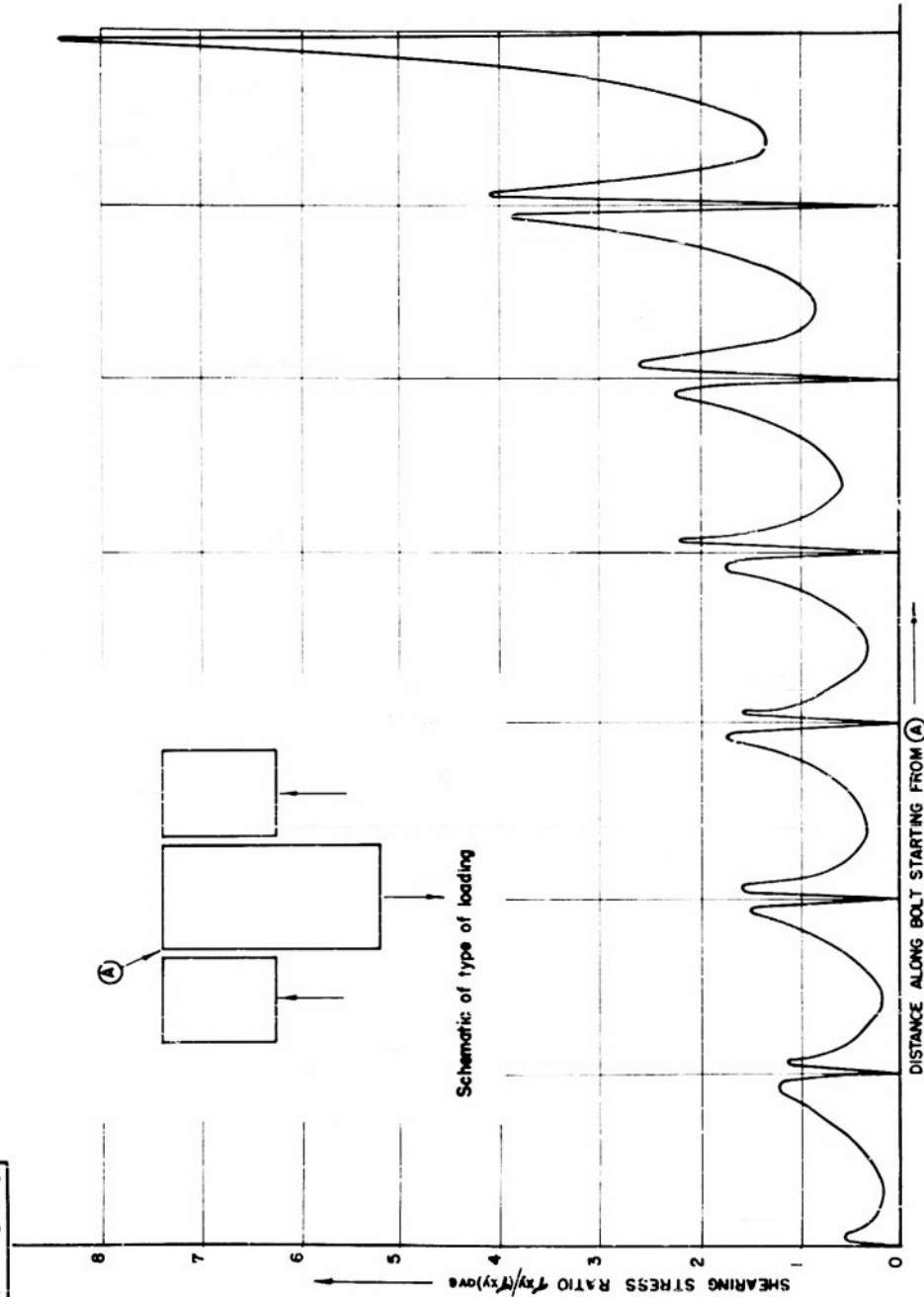
Fig. 8 Photoelastic Pattern at the Thread Root as Obtained
 Using the Petrographic Microscope
 (See Root A in Fig. 6 a)

A typical distribution of shear stress along the base of the threads is shown in Drawing No. P-438-C. This corresponds to the data taken from one radial slice of the threads and therefore shows the stresses for threads 180° apart on the thread helix. The area under the curve of shear stress is a measure of the total shearing force carried by each tooth of the thread. The high values of shear stress are of interest and indicate the influence of the stress raisers near the roots of the threads. In Drawing P-439-C similar results are shown for the model with tapered bolt diameter.

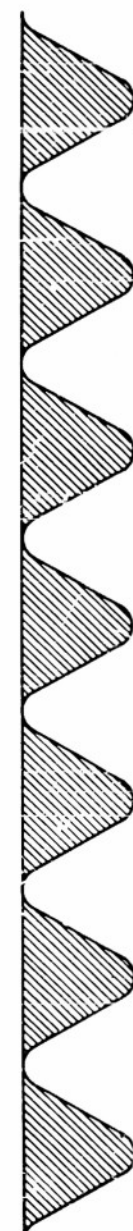
The experimental results are shown in graphical form in Drawings No. P-440-B and P-441-B. In addition the theoretical distribution of load along the thread helix is shown for two values of the coefficient of friction, which was not known precisely. Upon comparing the experimental points with the theoretical curves, it will be observed that the experimental results agree quite well with theory. Some discrepancies do exist, and probably arise due to the model being inaccurately machined. It is obvious that very slight errors in machining, particularly in the pitch and diameter of the threads, would lead to quite high localized effects.

The experimental results serve to emphasize the fact that in the preceding analysis for load distribution the shear stress across the base of the tooth plays an important role. It remains to be determined if a similar analysis can be introduced which will lead to a simple and accurate evaluation of the maximum normal stress in the threads. Once such a procedure is established, the design of threaded connections will become a straight forward process.

P-438-C



DISTANCE ALONG BOLT STARTING FROM (A)



ALTERATIONS

MARK	DESCRIPTION	BY	DATE	APPROVED

GENERAL NOTES

1. SHEARING STRESSES ALONG BOLT TYPE TREADS COMPUTED FROM PHOTOELASTIC MEASUREMENTS FOR AXIAL SLICE #3.7
2. $(\tau_{xy})_{avg} = P/2\pi D_0$

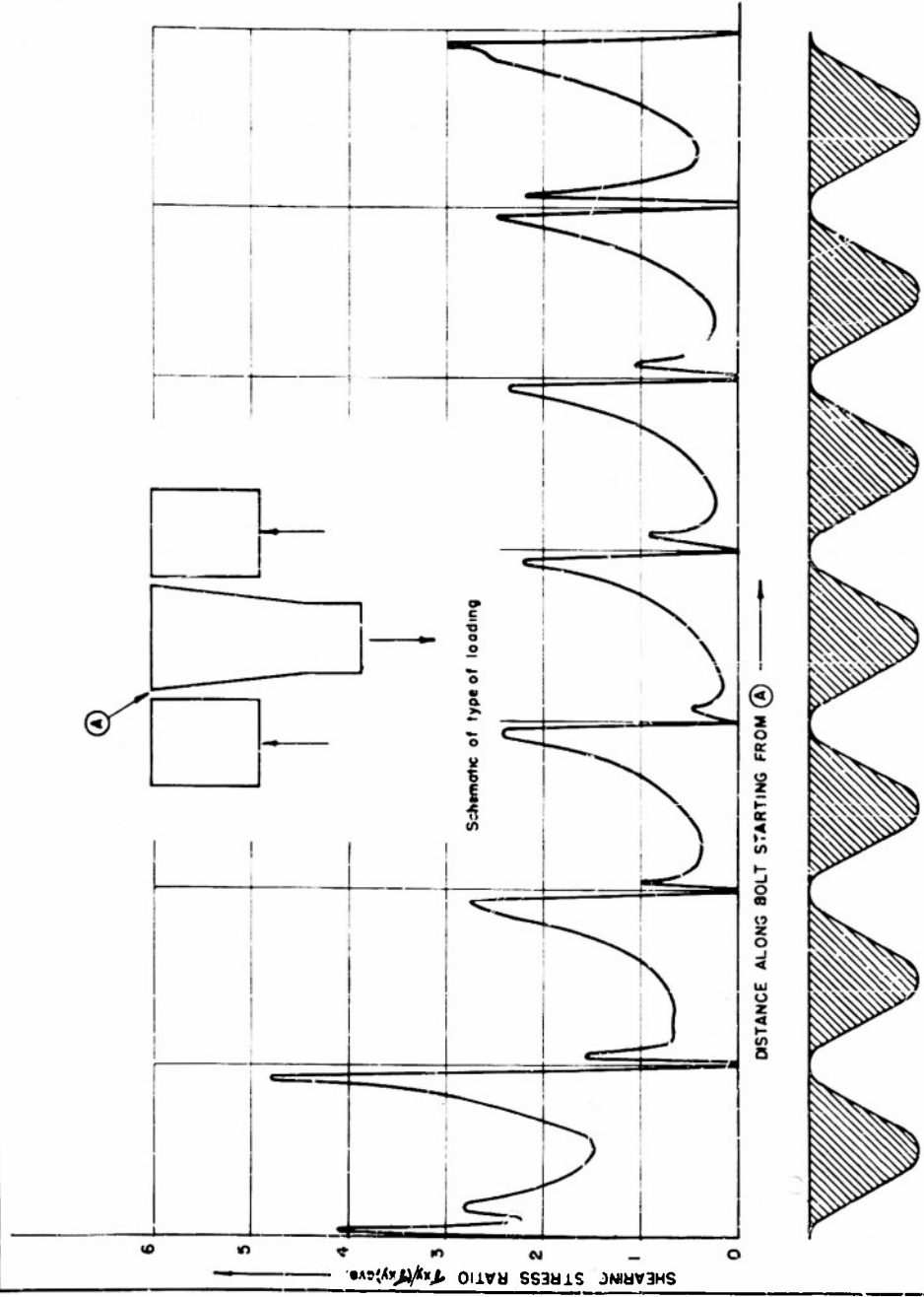
REFERENCES

ENGINEERING MECHANICS
LABORATORY
PURDUE UNIVERSITY
PROJECT

NON-TAPERED THREAD
SHEAR STRESS DISTRIBUTION

DESIGNED BY: SCALE: DATE: 2-18-34
DRAWN: L.P. CHECKED: J.A. APPROVED: J.A.
P-438-C

P-439-C



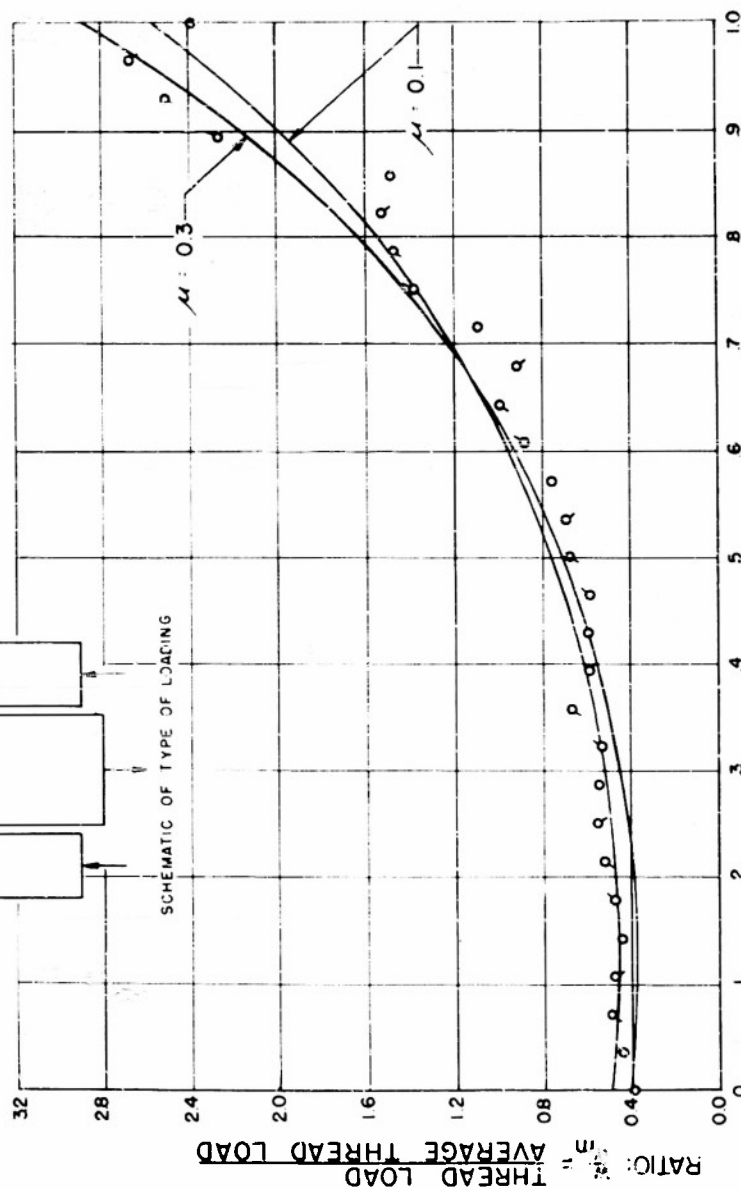
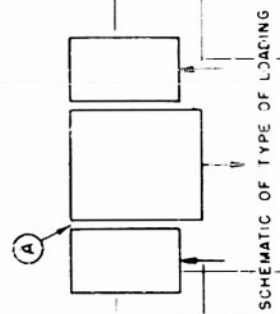
ALTERATIONS		
MARK	DESCRIPTION	BY DATE APPD

GENERAL NOTES
 1. SHEAR STRESSES ALONG BASE OF THREADS COMPUTED FROM PHOTOELASTIC MEASUREMENTS FOR AXIAL STRESS NO. 5.
 2. $\sigma_{max} = 10/3 \sigma_{avg}$

REFERENCES

ENGINEERING MECHANICS LABORATORY PURDUE UNIVERSITY PROJECT	
TAPERED THREAD SHEAR STRESS DISTRIBUTION	
DESIGNED BY C.	SCALE
DRAWN BY	DATE 5-22-54
CHECKED BY	APPROVED
P-439-C	

P-440B



ALTERATIONS		
MARK	DESCRIPTION	BY DATE APPD

GENERAL NOTES

1. EXPERIMENTAL POINTS OBTAINED FROM PHOTOELASTIC MEASUREMENTS.
 a SLICE NO. 8.
 b SLICE NO. 6.
 c SLICE NO. 7.
 d SLICE NO. 5.

2. THEORETICAL CURVES FOR TWO VALUES OF COEFFICIENT OF FRICTION OBTAINED USING D G SOWMITH'S SOLUTION

REFERENCES

1. DRAWING NO. P-438-C

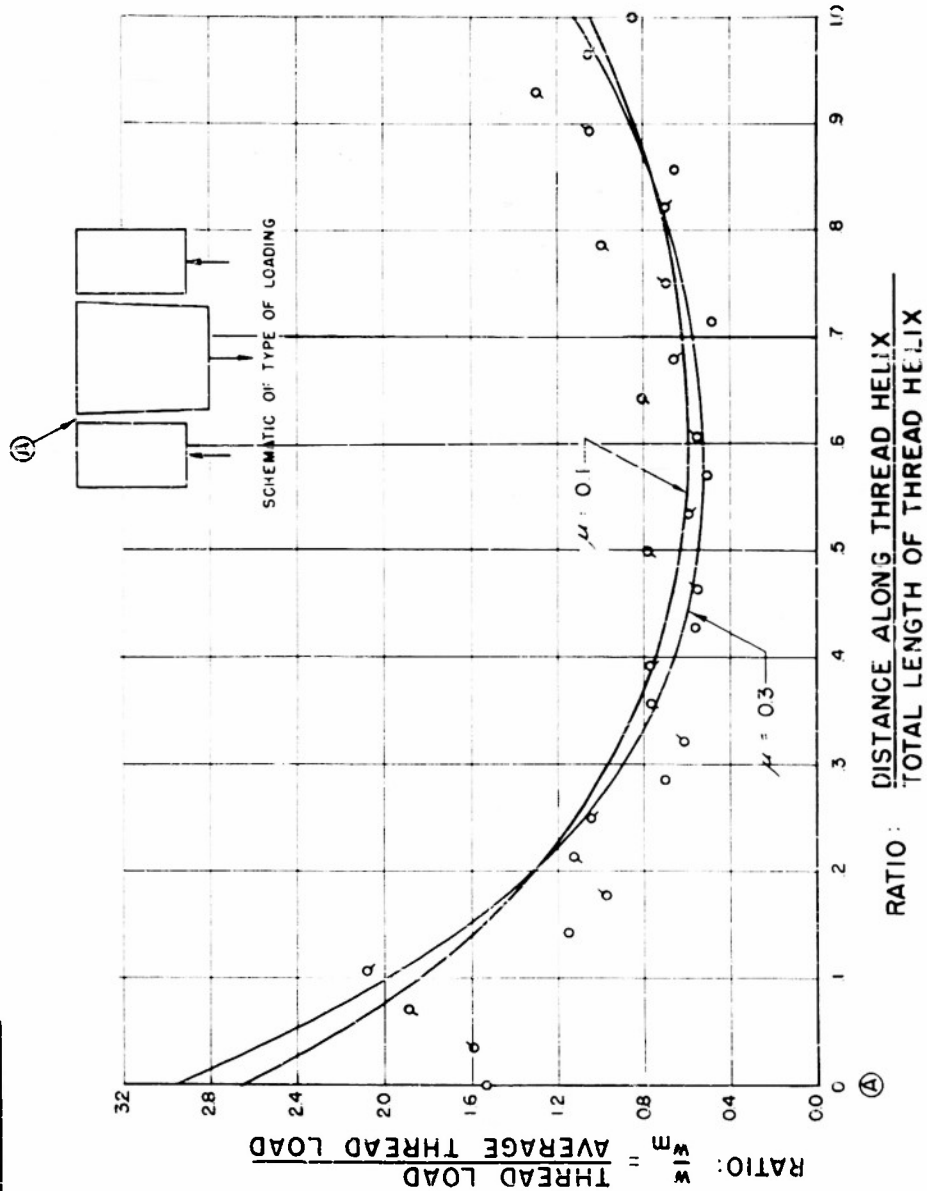
**ENGINEERING MECHANICS
LABORATORY**
 PURDUE UNIVERSITY
 PROJECT C 71

**NON-TAPERED THREAD
LOAD DISTRIBUTION**

DRAWN: R.M.G. DATE: 2-5-54
 CHECKED: J.M.G.
 APPROVED: J.M.G.

P-440-B

P-441-B



ALTERATIONS		
MARK	DESCRIPTION	BY DATE APPD

GENERAL NOTES

1. EXPERIMENTAL POINTS OBTAINED FROM PHOTOELASTIC MEASUREMENTS.

o SLICE NO. 1
 o SLICE NO. 2
 o SLICE NO. 3
 o SLICE NO. 4

2. THEORETICAL CURVES FOR TWO VALUES OF COEFFICIENT OF FRICTION OBTAINED USING STOCKLEY AND MACKE SOLUTION.

REFERENCES

1. DRAWING NO. P-439-C

**ENGINEERING MECHANICS
LABORATORY**
 PURDUE UNIVERSITY
 PROJECT C-71

**TAPERED THREAD
LOAD DISTRIBUTION**

DRAWN R.M.C.
 CHECKED *[Signature]*
 APPROVED *[Signature]*

DATE 2-5-54

P-441-B

CONFIDENTIAL

CONCLUSIONS

1. The theoretical results of Sopwith and Stoeckley and Macke can be extended to include different combinations of nut and bolt configurations. The analytic results of this study have been summarized for each independent permutation of loading for nuts and bolts of constant cross-section. Further theoretical work can be directed toward the problem of non-uniform cross-sections of nuts and/or bolts, including the effect of internal pressure when confined by non-uniform cross-sections.

2. It can be seen from the Drawings, Pages 20 to 22, that a change of the coefficient of friction from 0.1 to .3 does not greatly change the load distribution. As observed by Sopwith, however, improved lubrication tends to improve the load distributions.

In addition it also may be observed that, maintaining all other factors constant, decreasing the number of threads in engagement has a beneficial effect on the load distribution.

3. In the case of the models tested, the experimental results agree quite favorably with the theoretical. It would appear, therefore, that the theoretical analysis leads to a load distribution which is accurate; the deviations occurring seem to be due to local inaccuracies in machining.

Respectfully submitted,

Robert M. Gray
Robert M. Gray

July 1, 1954

APPROVED:

Paul F. Chenea
Paul F. Chenea
E. O. Stitz
E. O. Stitz

APPENDIX A

THE PETROGRAPHIC MICROSCOPE

The polarizing microscope, shown in Figure 9, was purchased to permit the more accurate evaluation of photoelastic data. Included in the microscope are all the necessary polariscope elements such as the polarizer, analyzer, and quarter wave plates. These are each shown in their operative positions in Figure 10. Provision was made to remove the two quarter wave plates from the field to form a crossed plane polariscope and thus to permit the determination of isoclinics or stress directions. In addition, the analyzer is rotatable through ninety degrees and, with the crossed circular arrangement of the elements, partial fringe orders may easily be determined using the Tardy method.

Two light sources are available for use with the microscope. One is a standard white light source for use in determining stress directions, and the second is a mercury vapor lamp matched to the quarter wave plates for determining fringe orders. In addition, a photomicrographic camera may be employed for photographing the fringe patterns. (See Figure 9) A calibrated mechanical stage, attached to the rotating stage of the microscope, and having two degrees of translation at right angles to one another, permits translatory movement of the model.

During operation, the model (generally a slice from a three-dimensional model with frozen-in stresses) is placed in a small oil bath having a glass bottom, which in turn is mounted upon the mechanical stage. The oil bath minimizes the diffusion of light at the unpolished surfaces of the slice, and both isoclinics and fringes are more clearly defined as a result. Once the model has been aligned in the oil bath, the location of specific points in the model is easily accomplished using the stage micrometer.

The chief advantages of the polarizing microscope over a conventional polariscope are the finer definition of both fringes and isoclinics. While the image of the model is magnified, the fringes and isoclinics appear as very narrow bands under the polarizing microscope. Thus it is less difficult to interpolate to the exact center of the isoclinic bands and fringes. In the author's opinion, the isoclinic parameters can be obtained accurately to 0.1 degree while the partial fringes may be read to within 0.01 fringes, particularly in regions of

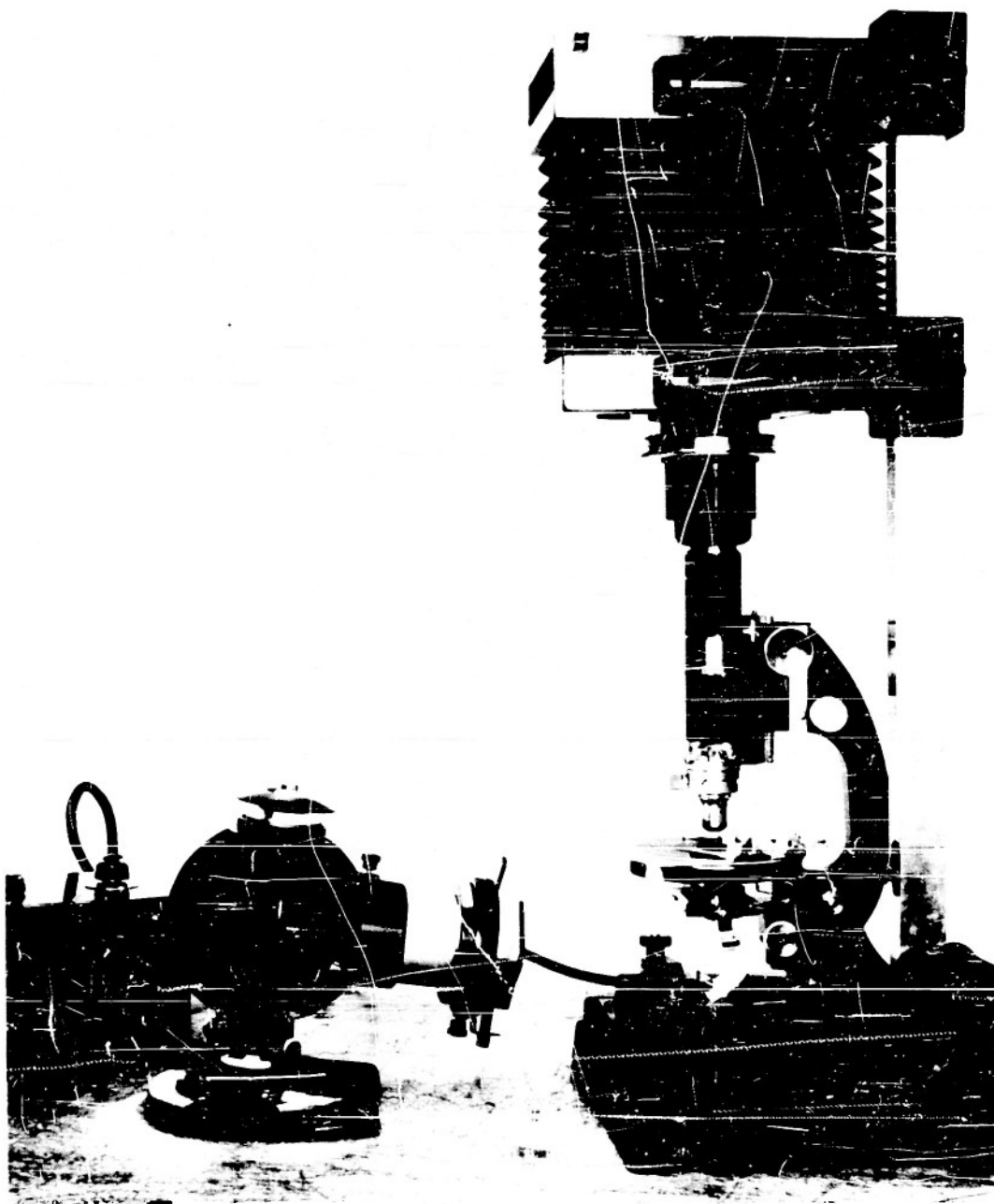


Figure 9

Petrographic Microscope Shown With Camera and 5461A^o
Light Source

Analyzer

Slide Mount for
2nd Quarter Wave Plate

Mechanical
Stage

Lever for 1st
Quarter Wave Plate

Polarizer

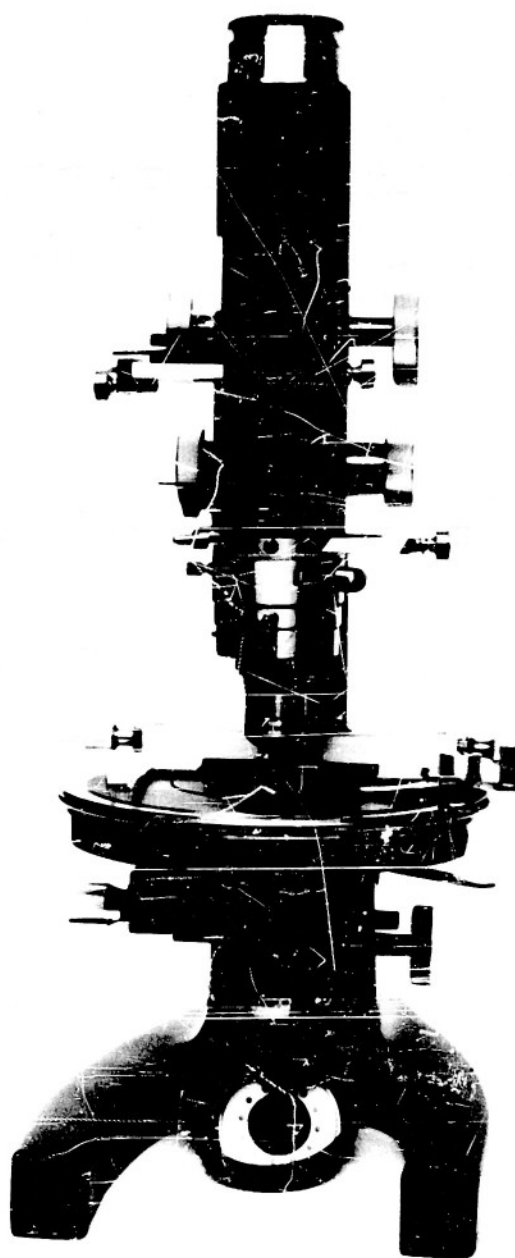


Fig. 10 Special Petrographic Microscope

high gradient of stress. A further advantage lies in the speed with which several successive readings can be made. Instead of aligning the polariscope to the model, the model is rotated relative to the polariscope and requires fewer manual operations. It is estimated that as many as ten readings can be made using the polarizing microscope during the time required for one reading using the conventional polariscope.

The advantages of the polarizing microscope become of greater importance in view of recent developments in photoelasticity. The trend is in the direction of low stressed models and consequent low fringe orders to avoid excessive distortion of the model. In such cases the fringe orders are low and the partial fringes must be accurately evaluated at several points in order to obtain a good extrapolation curve. For highly stressed models such a procedure is not necessary, since the fringe orders are generally high enough that several points on an extrapolation curve can be obtained using only the integral and half-order fringes (black and white background photographs respectively).

BIBLIOGRAPHY

1. Sopwith, D. G., "The Distribution of Load in Screw Threads", Proceedings, Institution of Mechanical Engineers, vol. 159, 1948, pp. 373-83, 396-7.
2. Stoeckley, E. E. and Macke, H. J., "Effect of Taper on Screw Thread Load Distribution", Transactions of the American Society of Mechanical Engineers, vol. 74, number 1, Jan. 1952, pages 103-12.
3. "Notes on a Screw Thread Program," by Applied Mechanics Branch, Watertown Arsenal Laboratory
4. Report B 1.1 - 1949, "The New American Standard Unified and American Screw Threads for Screws, Bolts, Nuts, and Other Threaded Parts", by ASA Sectional Committee B 1, sponsored by ASME and SAE.

AD

CLASSIFICATION CHANGED

FROM **CONFIDENTIAL** TO **UNCLASSIFIED**

43214

ON 2 March 1955 By authority of Reclass. Bull. List No. 17
Month Day Year Specify Authority being used

This action was rendered by Arthur C. Creech OSA
Name in full Date

Document Service Center, ASTIA

UNCLASSIFIED

UNCLASSIFIED